CWP-116
May 1992

A Dip-Dependent Divergence Correction

Francesca Fazzari

— Master of Science Thesis —
Geophysical Engineering

Center for Wave Phenomena
Colorado School of Mines
Golden, Colorado 80401
(303) 273-3557

ABSTRACT

A divergence correction is conventionally applied to zero-offset data in an effort to preserve amplitude information. The conventional divergence correction compensates for the geometrical spreading of a point source in a horizontally layered medium where velocity varies with depth only. The dip-dependent divergence correction extends the conventional correction for improved amplitude processing of dipping beds.

The dip-dependent divergence correction is computed by dynamic ray tracing, and applied to stacked data using a dip decomposition technique. This correction decreases amplitudes relative to the conventional correction for steep dips and late times. In a data example from the Gulf of Mexico, the conventional correction over-amplified the reflection off a salt dome flank by a factor of 1.6.

High amplitudes near salt flanks are also associated with the presence of hydrocarbons. Applying the dip-dependent divergence correction ensures that 'bright spots' are not due to over-amplification of steep dips by the conventional correction.

In areas like the Gulf of Mexico, where the velocity function varies primarily with depth, and steep beds are commonplace, the dip-dependent divergence correction is an inexpensive way to improve the amplitude information in seismic images.

INTRODUCTION

Divergence correction is applied to compensate for the decay in amplitude due to the geometrical spreading of the wavefront generated by a seismic source. One purpose of the dip-dependent divergence correction is to compensate for the geometrical spreading along a normal-incidence raypath to a *dipping* reflector. As well, dip-dependent divergence correction is designed to render zero-offset data consistent with the exploding reflector model (Loewenthal, et al., 1976). After dip-dependent divergence-correction and migration with an exploding reflector scheme, amplitudes are more interpretable in terms of the interface reflection coefficients.

Consider the geometrical spreading along a raypath that corresponds to a particular seismic event in either zero-offset, or finite offset data. The divergence correction for a particular reflection depends upon the location of the subsurface reflection point relative to the source location, and upon the velocity function of the overburden.

Conventional and Dip-dependent Divergence Correction

For zero-offset reflections from horizontal beds in a $v(z)$ medium, where the velocity v varies only with depth z, the reflection point depends on the vertical traveltime of the seismic energy and the velocity of the medium. Traveltime and velocity therefore determine the zero-offset divergence correction for horizontal reflectors. Newman (1973) derived this correction – $v_{\text{rms}}^2 t/v_0$, where t is the two-way vertical traveltime to the reflector, v_0 is the velocity at the surface, and v_{rms} is the root-mean-square average velocity along the vertical path between surface and reflector.

Newman also derived the divergence correction for finite-offset reflections from horizontal reflectors in a $v(z)$ medium. Two-point ray tracing is not necessary to compute this offset-dependent divergence correction. To see this, consider a raypath associated with a finite-offset reflection from a horizontal bed. This raypath is symmetrical; i.e., incident and reflected raypaths are characterized by a single value of the horizontal slowness (reflection slope), which is constant along a ray in a $v(z)$ medium. As well, the traveltime of each raypath is equal to one-half the reflection time. Both horizontal slowness (reflection slope) and traveltime are obtainable from the finite-offset reflection which corresponds to this raypath. Given horizontal slowness and traveltime, a ray may be traced through the $v(z)$ medium, and thus the location of the reflection point and the divergence correction may be determined, without requiring *two-point* ray tracing.

For media with dipping and curved interfaces, other authors (e.g., Červený and Ravindra, 1971; Červený, et al., 1977) have employed asymptotic ray theory to determine a general expression for the wave amplitude, including the divergence term. Červený, et al., described how to evaluate this divergence correction in the ray-centered coordinate system using the dynamic ray tracing equations. The divergence correction for dipping and curved interfaces is computed by tracing rays through

the medium, and solving the dynamic ray tracing equations at every ray-centered coordinate.

The finite-offset divergence correction for a reflection from a dipping reflector in a $v(z)$ medium is therefore determined by tracing both incident and reflected rays. A finite-offset raypath to a dipping reflector is not symmetrical. Horizontal slowness and traveltime along the incident raypath to a reflection point on a dipping reflector differ from those along the reflected raypath. Traveltime along incident and reflected raypaths cannot be determined directly from the reflection time of the corresponding event. Two-point ray tracing is required to determine these traveltimes, as well as the horizontal slownesses of the incident and reflected raypaths. Once these quantities have been computed, the divergence correction for reflections from dipping beds in finite-offset data may be computed as described by Červený, et al.

In this thesis, I use the dynamic ray tracing equations to determine the zero-offset divergence correction for any reflector in a medium where velocity varies with depth only. For stacked data, the dip-dependent divergence correction is applied without the computational cost of two-point ray tracing. To see this, consider a raypath normally incident to a reflection point. This raypath is characterized by a single value of the horizontal slowness (reflection slope) and a single traveltime, which is one-half of the reflection time of the corresponding zero-offset event. From the reflection time and reflection slope of this event, the normal-incidence ray may be traced. The zero-offset divergence correction may therefore be determined *without* two-point ray tracing.

Exploding Reflector Migration

After stack and divergence correction, seismic data are migrated. When divergence correction is applied, amplitudes of zero-offset dipping reflections are properly processed for amplitude decay due to geometrical spreading and should become more interpretable in terms of the interface reflection coefficients. This improvement in amplitude processing, however, is often negated by subsequent application of a migration scheme.

For migration processes based on the exploding reflectors concept (Loewenthal, et al., 1976), amplitude errors arise from two sources: incorrect treatment of the amplitude term in the solution to the acoustic wave equation, and *differences* between the assumed exploding reflector data and the actual stacked data. For example, the commonly used phase-shift migration (Gazdag, 1978) is based on a solution to the wave equation that includes no amplitude term at all. Reverse time migration (Baysal, et al., 1983), however, correctly processes the amplitudes for an exploding reflector source by simply running the acoustic wave equation backwards in time.

The amplitude error associated with reverse time migration results from the difference between exploding reflector and zero-offset data. The dip-dependent divergence correction is designed to compensate for this difference.

Exploding Reflector Correction

In the exploding reflector model, every interface reflection point in the subsurface explodes simultaneously, with source strength proportional to the reflection coefficient at that point. Consider a curved exploding reflector (Figure 1). When every surface element along that reflector explodes at the same time, this generates a wavefield that travels from the reflector up to the receiver. The raypaths perpendicular to the upgoing wavefield are identical to the reflected, upgoing segments of the normal-incidence raypaths.

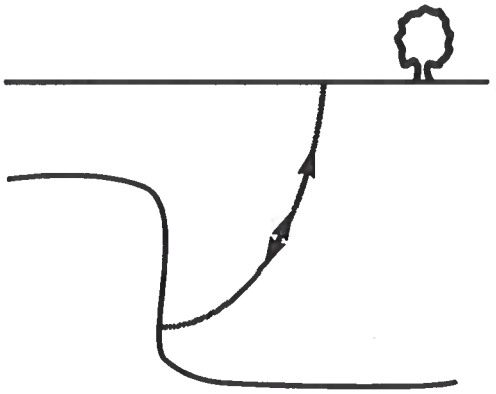

FIG. 1. Curved reflector with structure that approximates a salt flank. An exploding reflector raypath is indicated by the single arrow, and a normal-incidence raypath by the double arrows.

The amplitudes in zero-offset data ZO will be diminished by geometrical spreading GS_{down} along the raypath from source to reflection point as well as geometrical spreading GS_{up} along the raypath from reflection point to receiver,

$$ZO \propto GS_{down} \times GS_{up}.$$

The amplitudes in exploding reflector data ER decay due to geometrical spreading GS_{up} only along the raypath from reflection point to receiver,

$$ER \propto GS_{up}.$$

To account for the difference between exploding reflector and zero-offset data, the divergence correction must multiply zero-offset data by the reciprocal of the geometrical spreading GS_{down} along the raypath from source to reflector.

This defines the dip-dependent divergence correction. It corrects for geometrical spreading along the *downgoing* normal-incidence raypath to a reflection point on a dipping reflector. After dip-dependent divergence correction, the amplitudes of zero-offset data conform to the exploding reflector model. Thus migration schemes based on this model will migrate dipping reflections without introducing amplitude error.

Note that the dip-dependent divergence correction preserves the amplitude information in the stack. Both the divergence correction and the exploding reflector migration that it complements are based on the assumption that reflections in the stack correspond to normal-incidence raypaths. Reflections from dipping beds require NMO and DMO processing before stack for that assumption to remain valid. Any amplitude errors introduced by pre-stack processing or the stacking process itself will be propagated by dip-dependent divergence correction and migration.

The poststack dip-dependent divergence correction is comparable to Newman's divergence correction. However, the conventional correction accounts for both downgoing and upgoing geometrical spreading. For comparison with the dip-dependent correction, the conventional correction is modified to account for geometrical spreading only from source to reflection point. Whereas the dip-dependent divergence correction properly compensates for point source spreading in reflections from dipping beds, the modified conventional correction *over-amplifies* reflections from dipping beds. (See the section on Divergence Correction Ratio, p. 19.)

In this thesis, I show how to derive the poststack dip-dependent divergence correction, and discuss its computer implementation. I show the results of applying the dip-dependent correction for a synthetic data example, and for a field data example from the Gulf of Mexico.

DERIVATION OF THE AMPLITUDE CORRECTION FACTOR

Divergence is one factor in the amplitude term of the ray series solution to the wave equation. The dip-dependent divergence *correction* is the inverse of this factor. The amplitude term varies depending on whether the constant density or constant impedance acoustic wave equation is used. I review the derivation of the amplitude term (e.g., Bleistein, 1984; Aki and Richards, 1980) from the transport equation for both constant density and constant impedance cases, because reverse time exploding reflector migrations implement *either* the constant density *or* the constant impedance acoustic wave equation. I show how the dynamic ray tracing equations are used to compute the divergence (e.g., Červený and Hron, 1980; Hubral, 1983), and the dip-dependent divergence correction. For horizontal reflectors, I show that the dip-dependent correction reduces to the conventional divergence correction, $v_{rms}^2 t/v_0$ (Newman, 1973). Finally, I discuss the factor by which the constant density amplitude differs from the constant impedance amplitude, and its implications for the dip-dependent divergence correction.

The Transport Equation and the Eikonal Equation

Divergence correction in this thesis is based on traveltimes and amplitudes computed along a ray. Upon substitution of the ray series solution into the constant density acoustic wave equation (e.g., Červený and Ravindra, 1971), traveltime and amplitude are solutions of separate equations, the eikonal equation (1) and the transport equation (2), respectively. For a medium where velocity varies with depth z only, the eikonal and the leading order transport equations are

$$\nabla t(\mathbf{x}) \cdot \nabla t(\mathbf{x}) - \frac{1}{v^2(z)} = 0; \tag{1}$$

$$2\nabla t(\mathbf{x}) \cdot \nabla A_0(\mathbf{x}) + A_0(\mathbf{x})\nabla^2 t(\mathbf{x}) = 0. \tag{2}$$

Both traveltime t along a ray and the leading order amplitude A_0 are functions of the three-dimensional Cartesian position vector $\mathbf{x}$. The eikonal equation relates the traveltime gradient ∇t, which points in the direction of the ray, to the velocity function $v(z)$.

The solution to the transport equation (2) describes the leading-order amplitude A_0. The ray series solution to the wave equation is an infinite series in inverse powers of frequency ω. For seismic data with three-dimensional geometrical spreading losses, the series may be approximated by the leading order term, which is the coefficient of the zeroth inverse power of frequency, $1/\omega^0$. When the velocity gradient is small with respect to the frequency (e.g., Červený and Ravindra, 1971, p. 22–23), the leading order term dominates the ray series. This condition is generally satisfied in reflection seismic data.

If the *constant impedance* acoustic wave equation for a $v(z)$ medium is used, substitution of the ray series solution results in an additional term in the transport

equation. The eikonal and the leading-order transport equations resulting from the *constant impedance* acoustic wave equation are

$$\nabla t(\mathbf{x}) \cdot \nabla t(\mathbf{x}) - \frac{1}{v^2(z)} = 0; \tag{3}$$

$$2\nabla t(\mathbf{x}) \cdot \nabla A_0(\mathbf{x}) + A_0(\mathbf{x})\nabla^2 t(\mathbf{x}) + \left[\frac{A_0(\mathbf{x})}{v(z)}\right] \nabla v(z) \cdot \nabla t(\mathbf{x}) = 0. \tag{4}$$

The Ray Tracing Equations

The solution to the eikonal equation determines the position of a ray as a function of traveltime along the ray and initial direction of the ray. The three dimensional slowness vector $\mathbf{p}$ is defined such that

$$\nabla t(\mathbf{x}) \equiv \mathbf{p}(\mathbf{x}) = p\hat{\mathbf{s}} = \frac{\hat{\mathbf{s}}}{v(z)},$$

where $\hat{\mathbf{s}}$ denotes a unit vector pointing in the direction of the ray. The magnitude p of the slowness vector $\mathbf{p}$ is thus equal to $1/v(z)$.

The eikonal equation (1) involves the dot product of the gradient of traveltime t, and is non-linear in t. A standard approach to solving such non-linear partial differential equations is the method of characteristics (e.g., Bleistein, 1984, p. 1–18). Applying the method of characteristics to the eikonal equation yields the ray tracing equations

$$\frac{dx_i}{dt} = \frac{p_i}{p^2}, \qquad \frac{dp_i}{dt} = \frac{1}{p}\frac{\partial p}{\partial x_i}, \tag{5}$$

where the subscript i refers to one of the three Cartesian coordinate directions (x_1, x_2, x_3). Using equations (5), rays may be traced through the $v(z)$ medium.

Solution of the Transport Equation

The left-hand side of the transport equation (2) is equivalent to the divergence of $A_0^2\nabla t$. Integrating both sides of this equation over a volume V and applying Gauss's law, $\int_V \nabla \cdot \mathbf{f}\ dV = \int_S \mathbf{f} \cdot \hat{\mathbf{s}} dS$, yields

$$\int_S A_0^2(\nabla t \cdot \hat{\mathbf{s}}) dS = 0, \tag{6}$$

where $\hat{\mathbf{s}}$ now denotes the normal to the surface S, and dS is a differential surface element. For S equal to the surface of a *ray tube*, every differential surface element dS has a unit normal either parallel or perpendicular to ∇t.

Traveltime t along the ray is used to track the ray's propagation and describe the ray tube. Consider a central ray and a family of nearby rays. The endpoints of the

family of rays at t_1 sweep out some surface area S_1. At a later t_2, the same family of nearby rays will sweep out a different surface area S_2, because the distance between the nearby rays changes as the rays propagate through the medium. The two surfaces S_1 and S_2, and the cylindrical surface that connects them define the ray tube.

The surfaces S_1 and S_2 have unit normals $\hat{\mathbf{s}}$ parallel to ∇t. For the family of nearby rays that define the sides of the ray tube, every element of surface area on the cylindrical surface is tangent to the direction of the central ray. Consequently, the unit normal at every point on the cylindrical surface is perpendicular to ∇t.

In the integration of equation (6) over the ray tube, only the surfaces S_1 and S_2 contribute. The dot product $\nabla t \cdot \hat{\mathbf{s}}$ has magnitude $|\nabla t| = v^{-1}(z)$, but opposite sign, for S_1 and S_2. At S_1,the surface normal $\hat{\mathbf{s}}$ is antiparallel to the ray direction ∇t, while at S_2 the two vectors are parallel. In the limit as the ray tube collapses to the central ray, S_1 and S_2 are equal to the differential surface elements dS_1 and dS_2, and the integral (6) equals the integral over the surface areas at t_1 and t_2:

$$\frac{A_1^2 dS_1}{v_1} - \frac{A_2^2 dS_2}{v_2} = 0,$$

$$A_2 = A_1 \sqrt{\frac{dS_1}{dS_2}} \sqrt{\frac{v_2}{v_1}}. \tag{7}$$

A_2 and A_1 denote the leading order amplitudes at times t_2 and t_1 along a central ray. v_2 is the velocity at depth z_2 corresponding to time t_2, and v_1 is defined analogously. Recall that the ray has travelled farther at t_2 than at t_1.

The ratio of differential areas in equation (7) defines the geometrical spreading. For reasons discussed in Appendix A, I will refer to the velocity ratio term as the transmission factor. The amplitude A_2 is thus the product of A_1, the geometrical spreading factor GS, and the transmission factor T

$$A_2 \;=\; A_1 \times GS \times T, \tag{8}$$

where

$$GS = \sqrt{\frac{dS_1}{dS_2}}, \qquad T = \sqrt{\frac{v_2}{v_1}}.$$

Equation (7) is the solution to the transport equation (2) resulting from the *constant density* acoustic wave equation. Following the discussion above, the solution to the transport equation (4) resulting from the *constant impedance* acoustic wave equation may be derived.

The left-hand side of the transport equation (4) is equivalent to the divergence of $A_0^2 v \nabla t$. Applying Gauss's law to both sides of equation (4) and integrating over a ray tube as in the above discussion yields

$$\frac{A_1^2 v_1 dS_1}{v_1} - \frac{A_2^2 v_2 dS_2}{v_2} = 0,$$

$$A_2 = A_1\sqrt{\frac{dS_1}{dS_2}} = A_1 \times GS, \tag{9}$$

where the terms in equation (9) are defined as in equation (7). The solution to the transport equation (4) resulting from the *constant impedance* acoustic wave equation contains only the ratio of cross-sectional areas $\sqrt{dS_1/dS_2}$, and no transmission factor.

To determine the amplitude at any point along a central ray, requires an expression for the geometrical spreading GS in terms of traveltime (or distance) along a ray, and for the amplitude term of constant density wave equation (7), the transmission factor must be evaluated as well. From the ray tracing equations, the Cartesian coordinates of any point along a central ray may be determined and the transmission factor computed.

The Geometrical Spreading Term

The product of initial amplitude and geometrical spreading may be written as the Jacobian of the transformation from Cartesian coordinates to ray coordinates (Bleistein, 1984, p. 260–270).

$$A_1\sqrt{\frac{dS_1}{dS_2}} = \sqrt{\frac{1}{J(s,\gamma_1,\gamma_2)}},$$

where the Jacobian $J(s,\gamma_1,\gamma_2)$ of the transformation between Cartesian and ray coordinates is defined by

$$J(s,\gamma_1,\gamma_2) \equiv \left|\frac{\partial(x_1,x_2,x_3)}{\partial(s,\gamma_1,\gamma_2)}\right|.$$

Ray coordinates are described by distance s along a ray, the ray's initial polar angle γ_1, and its initial azimuthal angle γ_2. Figure 2 illustrates the angular variables γ_1 and γ_2.

The Jacobian $J(s,\gamma_1,\gamma_2)$ measures the geometrical spreading due to a point source when the energy has travelled through the medium without reflection or refraction from an interface. The Jacobian $J(s,\gamma_1,\gamma_2)$ reduces to the product of two independent components: an in-plane component, and an out-of-plane component(e.g., Červený and Hron, 1980; Bleistein, 1986), when the point source amplitude is recorded on a seismic line oriented in the direction of geologic dip.

Recorded data from such a line corresponds to rays with initial direction parallel to the seismic line. It is convenient to orient the Cartesian system so that the seismic line lies along the $x_1 = x$ axis. Initial direction parallel to the x axis is thus equivalent to $\gamma_2 = 0$. Rays characterized by $\gamma_2 = 0$ are constrained to travel within the in-plane depth slice beneath the seismic line. A depth slice perpendicular to the seismic line lies in the out-of-plane direction.

For a seismic line at the surface of a $v(z)$ medium oriented in the direction of geologic dip, the three-dimensional Jacobian $J(s,\gamma_1,\gamma_2)$ is the product of the in-plane component $J_{\|}$ evaluated at $\gamma_2 = 0$, and the out-of-plane component σ. The

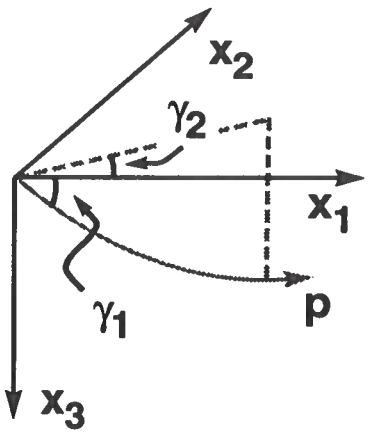

FIG. 2. γ_1 and γ_2 are defined with respect to a central ray shot from the origin of a Cartesian coordinate system (x_1, x_2, x_3).

three-dimensional spreading is therefore

$$\sqrt{\frac{1}{J(s,\gamma_1,\gamma_2)}} = \sqrt{\frac{1}{J_{\|}(s,\gamma_1,\gamma_2{=}0)\,\sigma(s,\gamma_1)}}.$$

The Jacobian $J_{\|}$ describes a coordinate transformation from the in-plane dimensions x, z, where depth $z{=}x_3$, to two-dimensional ray coordinates s, γ_1 $(\gamma_2{=}0)$

$$J_{\|} = \left|\frac{\partial(x,z)}{\partial(s,\gamma_1)}\right|.$$

$J_{\|}$ is computed using the dynamic ray tracing equations, as described in the following section.

Dynamic Ray Tracing Equations

Consider an in-plane raypath from shotpoint to subsurface reflection point (see Figure 3). The equations of dynamic ray tracing are based on the ray-centered coordinate system. In ray-centered coordinates, every point along a central ray has direction vector **s** and normal **n**. **s** and **n** define an orthogonal coordinate system at every point along the central ray. **s** has magnitude s equal to the distance travelled along the ray. The magnitude n of **n** is equal to the distance between the central ray (with angle γ_1) and a nearby ray (with angle $\gamma_1 + d\gamma_1$), when s is held fixed. The relationship of n to s is derived by expanding the eikonal equation about the central ray in the (s, n) coordinate system (Červený, 1981a)

$$\frac{dn}{ds} = vp_n, \qquad \frac{dp_n}{ds} = -\frac{v_{,nn}}{v^2}n. \tag{10}$$

These are the equations of dynamic ray tracing. p_n is the component of the slowness in the direction of the normal, and $v_{,nn}$ is the second derivative of velocity with respect to n.

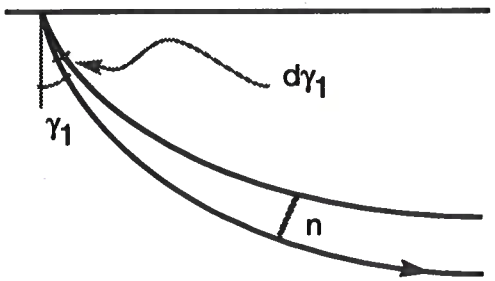

FIG. 3. The normal distance n at some distance s along the ray between a ray with take-off angle γ_1 and a nearby ray with take-off angle $\gamma_1 + d\gamma_1$. The initial normal distance is measured when the distance travelled along the ray is equal to unity. As both normal distances become small, the normal at s is approximated by the differential dn, and the initial normal distance by $1 \cdot d\gamma_1$ (Červený, 1981b). The ratio $d\gamma_1/dn$ is simply the ratio of the initial spreading to the spreading at distance s.

Equations (10) also describe the 2-D Jacobian $J_{||}$. $J_{||}(s, \gamma_1)$ is related to the Jacobian of the transformation between Cartesian and ray-centered coordinates $J(s, n)$ by the factor $\partial n/\partial \gamma_1$

$$\begin{aligned} J_{||}(s,\gamma_1) &= \left|\frac{\partial(x,z)}{\partial(s,\gamma_1)}\right| = \frac{\partial n}{\partial \gamma_1}\left|\frac{\partial(x,z)}{\partial(s,n)}\right| \\ &= \frac{\partial n}{\partial \gamma_1} J(s,n). \end{aligned} \tag{11}$$

As the ray tube collapses to the central ray, $J(s, n)$ approaches one (Červený, 1981b) and $J_{||}(s, \gamma_1)$ reduces to

$$J_{||}(s,\gamma_1) = \frac{\partial n}{\partial \gamma_1}. \tag{12}$$

$\partial n/\partial \gamma_1$ is evaluated by taking the partial derivative of the dynamic ray tracing equations (10) with respect to γ_1. Define q and p (Červený, 1981b) so that

$$q \equiv \frac{\partial n}{\partial \gamma_1} \qquad p \equiv \frac{\partial p_n}{\partial \gamma_1}.$$

In these new variables, the in-plane Jacobian $J_{||}(s, \gamma_1)$ is now simply q. The derivative of equations (10) with respect to γ_1 is

$$\frac{dq}{ds} = vp, \qquad \frac{dp}{ds} = -\frac{v_{,nn}}{v^2} q. \tag{13}$$

At $s = 0$, the nearby rays have not diverged from the central ray, and the in-plane spreading $q(s = 0)$ equals zero. For a source at the surface $z = 0$, where velocity

is v_0, initially, the partial derivative of normal slowness p_n with respect to γ_1 is proportional to $1/v_0$. The constant of proportionality is determined by the angle between the nearby rays and the central ray. For convenience, that constant is set to unity and $p(s=0) = 1/v_0$.

For a velocity function which varies with depth z only, $v_{,nn}$ is equal to $v_{,zz}p_x^2v^2$, where $v_{,zz}$ is the second derivative of velocity with respect to depth z, and p_x is the horizontal x component of the slowness $1/v(z)$ at any point along a raypath. Initially $p_x = \sin\gamma_1/v_0$. The dynamic ray tracing equations for the in-plane Jacobian q are

$$\frac{dq}{ds} = vp, \qquad \frac{dp}{ds} = -v_{,zz}\, p_x^2\, q. \tag{14}$$

In-plane and Out-of-plane Spreading

The in-plane Jacobian q is described by equations (14). When p in equations (14) is a constant, and equal to its initial value of $1/v_0$, the equation for q describes the out-of-plane spreading $\sigma(s,\gamma_1)$ (Bleistein, 1986)

$$\frac{d\sigma}{ds} = \frac{v}{v_0}, \tag{15}$$

where initially $\sigma = 0$. Like q, σ depends on the velocity along the path of the central ray, where the central ray is defined by a particular initial azimuthal angle γ_1. Horizontal slowness p_x may be used to characterize a central ray instead of the angle γ_1, because p_x is constant in a $v(z)$ medium, and $p_x(s=0) = \sin\gamma_1/v_0$. Instead of $\sigma(s,\gamma_1)$, the equivalent $\sigma(s,p_x)$ is used to describe the out-of plane spreading.

The dynamic ray tracing equations for the in-plane component of the spreading q and the out-of-plane component σ are

$$\begin{aligned} \frac{d\sigma}{ds} &= \frac{v}{v_0}; \\ \frac{dq}{ds} = vp, &\qquad \frac{dp}{ds} = -v_{,zz}\, p_x^2\, q. \end{aligned}$$

The product of initial amplitude and geometrical spreading may now be written

$$\begin{aligned} A_1\sqrt{\frac{dS_1}{dS_2}} &= \sqrt{\frac{1}{J(s,\gamma_1,\gamma_2)}}, \\ &= \sqrt{\frac{1}{\sigma q}}, \end{aligned} \tag{16}$$

where both σ and q are functions of distance s along a ray, and the horizontal component of the slowness p_x. Note that σ and q depend on velocity along the raypath. Velocity is a function of depth z; it may be computed at any point along the raypath

from the ray tracing equations (5), which are differential equations in *traveltime* t along the ray. I use the relation $ds = vdt$ to rewrite equations (14) in terms of the differential dt

$$\frac{d\sigma}{dt} = \frac{v^2}{v_0}; \tag{17}$$

$$\frac{dq}{dt} = v^2 p, \qquad \frac{dp}{dt} = -v_{,zz} p_x^2 v\, q\ , \tag{18}$$

where $\sigma(t=0)0$, $q(t=0) = 0$, and $p(t=0) = 1/v_0$.

Amplitude Correction

The constant density wave equation amplitude is given by equation (8). It is the product of initial amplitude, geometrical spreading GS, and transmission T. These quantities may be computed at any point along a ray using equations (18), (17), and the ray tracing equations (5). The initial velocity in the transmission factor is v_0, for I have assumed the point source was located at the surface $z = 0$. The velocity at some later time corresponding to depth z may be expressed as $v(z)$, where the mapping $z = z(t, p_x)$ is implicit. The amplitude at depth z is therefore

$$A(t, p_x; v) = \sqrt{\frac{1}{\sigma(t, p_x; v) q(t, p_x; v)}} \sqrt{\frac{v(z)}{v_0}}. \tag{19}$$

The amplitude correction D for a point source located at the surface, where amplitudes are observed at depth z is simply the reciprocal of the right hand side of equation (19)

$$D(t, p_x; v) = \sqrt{\sigma(t, p_x; v) q(t, p_x; v)} \sqrt{\frac{v_0}{v(z)}}. \tag{20}$$

The correction D is the dip-dependent divergence correction; it has an in-plane spreading component $\sqrt{q}$, and an out-of-plane spreading component $\sqrt{\sigma}$. The transmission correction $\sqrt{v_0/v(z)}$ is included in the dip-dependent divergence correction for the solution to the *constant density* acoustic wave equation (7), but not for the solution to the *constant impedance* acoustic wave equation (9).

The dip-dependent divergence correction D without transmission factor may be compared to the conventional divergence correction $v_{\text{rms}}^2 t'/v_0$ (Newman, 1973), where t' is reflection time. For rays normally incident upon a reflector, the reflector dip is equal to the angle θ between the ray and the vertical z axis. Because the horizontal slowness p_x at any point along a ray is given by $\sin\theta(z)/v(z)$, for horizontal reflectors, $p_x = 0$. The dip-dependent divergence correction D at $p_x = 0$ is

$$D(t, 0; v) = \sqrt{\sigma(t, p_x; v) q(t, 0; v)}. \tag{21}$$

When p_x is zero, p in equation (18) is a constant, equal to its initial value $1/v_0$. The dynamic ray tracing equations (18) for q and p reduce to a single equation,

$$\frac{dq}{dt} = p_0 v^2 = \frac{1}{v_0} v^2. \tag{22}$$

Equation (22) is identical to equation (17), the differential equation for σ. The solution of equations (17) for σ, and also q, may be written in integral form

$$\sigma = q = \frac{1}{v_0} \int_0^t v^2 dt = \frac{v_{\text{rms}}^2 t}{v_0}.$$

Substituting these results into equation (21), the divergence correction for horizontal reflectors is therefore

$$\begin{aligned} D(t, 0; v) &= \frac{v_{\text{rms}}^2 t}{v_0}, \\ &= \frac{v_{\text{rms}}^2 t'}{2v_0}. \end{aligned} \tag{23}$$

Because equation (23) depends on traveltime t along the raypath to the reflection point, it is actually half of the conventional correction. The conventional correction is proportional to two-way reflection time, or *twice* the traveltime to the reflection point for a normal-incidence raypath.

Transmission Factor

The dip-dependent divergence correction is applied to correct zero-offset data so that amplitudes are consistent with the exploding reflector model. The combination of dip-dependent divergence correction followed by migration, will improve the diagnostic value of the amplitude information in the stack. As discussed previously, the migration process must treat amplitudes in accordance with the acoustic wave equation, as does reverse time migration. If the migration scheme is based on the constant density acoustic wave equation, amplitudes after divergence correction will be consistent with exploding reflector data, *only* if the transmission factor is included. To see this, compare a zero-offset amplitude associated with a particular reflection point to the exploding reflector amplitude associated with the same point.

In its most general form, the *constant density* amplitude, equation (8), is the product of initial amplitude A_1, geometrical spreading GS, and transmission factor T

$$A_2 = A_1 \times GS \times T = GS \times \sqrt{\frac{v_2}{v_1}},$$

where A_2 is the amplitude at some depth z_2, v_2 is the velocity at depth z_2, and v_1 is the initial velocity. For a zero-offset reflection from a reflector at depth z where the

velocity is $v(z)$, amplitude is proportional to

$$\begin{aligned} A &\propto GS_{down} \times \sqrt{\frac{v(z)}{v_0}} \times GS_{up} \times \sqrt{\frac{v_0}{v(z)}} \\ &\propto GS_{down} \times GS_{up}. \end{aligned}$$

The recorded amplitude A is the product of geometrical spreading GS_{down} along the downgoing raypath, the downgoing transmission $\sqrt{v(z)/v_0}$, where v_0 is the velocity at the surface, geometrical spreading GS_{up} along the upgoing raypath, and upgoing transmission $\sqrt{v_0/v(z)}$. The transmission factor is equal to unity along the normal-incidence raypath that originates from and returns to the source depth $z=0$. If that same reflector at depth z was an exploding reflector, then the recorded amplitude would be proportional to

$$A \propto GS_{up} \times \sqrt{\frac{v_0}{v(z)}}.$$

So that zero-offset amplitudes are consistent with exploding reflector amplitudes, the dip-dependent divergence correction D must correct for both geometrical spreading and the transmission factor along the downgoing normal-incidence raypath

$$D = \frac{1}{GS_{down} \times \sqrt{v(z)/v_0}} = \frac{1}{GS_{down}} \times \sqrt{\frac{v_0}{v(z)}}.$$

Reverse time migration based on the *constant density* acoustic wave equation will account for transmission and geometrical spreading while running the wave equation backwards in time. For an event recorded from a reflector at depth z, the reverse time migration will *back out* the upgoing divergence GS_{up}, as well as the upgoing transmission $\sqrt{v_0/v(z)}$. However, zero offset amplitudes do not include the factor $\sqrt{v_0/v(z)}$. The dip-dependent divergence correction must multiply zero-offset amplitudes by the transmission factor $\sqrt{v_0/v(z)}$, so that the migration scheme processes amplitudes correctly.

To properly process amplitudes, reverse time migration schemes that rely on the constant density acoustic wave equation must include the transmission factor $\sqrt{v_0/v(z)}$ with the dip-dependent divergence correction. If, however, the migration is based on the non-reflecting or constant-impedance acoustic wave equation (Baysal, et al., 1984), the transmission factor drops out of the amplitude as in equation (9). Constant impedance amplitude A_2 at depth z_2 depends only on initial amplitude A_1 and geometrical spreading GS

$$A_2 = A_1 \times GS.$$

Only spreading correction is required to make zero-offset amplitudes consistent with the exploding reflector model. For reverse time migrations that use the non-reflecting

wave equation, such as the migration applied in the data examples (the section on Results, p. 27), the transmission factor $\sqrt{v_0/v(z)}$ should not be included.

IMPLEMENTATION

In this section, I discuss the computational methods used to implement the post-stack dip-dependent divergence correction. The differential equations (18) and (17) that determine components σ and q of this correction are solved numerically using finite differences. σ, q, and the divergence correction are determined for the range of reflection slopes and reflection times found in the recorded data. I then describe the dip-decomposition technique used to apply the dip-dependent divergence correction to zero-offset data.

The dip-dependent divergence correction corrects for the amplitude loss due to geometrical spreading along the raypath from source to reflection point. The dip-dependent divergence correction, without the transmission factor is

$$D(t,p_x;v) = \sqrt{\sigma(t,p_x;v)q(t,p_x;v)},$$

where σ and q are defined by the differential equations (17) and (18). By solving these equations for σ and q, the dip-dependent divergence correction can be tabulated for all downgoing traveltimes t and all horizontal slownesses p_x.

To apply the dip-dependent divergence correction to stacked data, it must be tabulated not as a function of downgoing traveltime and horizontal slowness, but as a function of two-way reflection time and reflection slope of zero-offset data. By halving the interval-velocity function v, the divergence correction to the reflection point is computed for all *reflection* times t. Horizontal slowness $p_x = \sin\theta(z)/v(z)$, where θ is the angle between the ray, and the vertical z axis is equal to one-half the reflection slope on a zero-offset section. Again, by halving the velocity, the dip-dependent divergence correction for the normal-incidence raypath from source to reflector can be tabulated for all reflection slopes p_x. For a given zero-offset section, values of p_x range from 0 to the maximum reflection slope, $2/v_0$.

Numerical Solution for σ and q

The finite difference solution to the equations for σ and q marches forward in reflection time t, for all possible values of the reflection slope p_x. Recall that for a $v(z)$ medium, the horizontal slowness is a constant along the ray. For a particular reflection slope p_x, marching forward in reflection time is equivalent to tracing normal-incidence rays to reflectors of different dip and depth.

The forward difference approximation to σ, equation (17), results in

$$\sigma^{j+1} = \sigma^j + \frac{\Delta t}{v_0}\left[v(j\Delta t)\right]^2,$$

where σ^j represents $\sigma(j\Delta t;v)$, $\sigma^0 = 0$, and Δt is the time sampling interval. Implicit in the notation $v(j\Delta t)$, is a mapping from reflection time t to depth z. This mapping is given by the ray equation (5) for depth z

$$\frac{dz}{dt} = \frac{p_z}{p_x^2 + p_z^2} = v^2 p_z, \tag{24}$$

where p_z is the vertical component of the slowness $1/v(z)$. When $p_x = 0, p_z = 1/v(z)$, the right side of equation (24) reduces to $v(z)$, and reflection time t along the ray is equivalent to vertical time τ, which is used as the independent variable in seismic field velocities.

The forward finite difference approximations to equations (18) deliver values that oscillate in an unphysical manner when the curvature of the velocity function $v_{,zz}$ changes sign rapidly. I removed this instability by using a simple implicit scheme, the Crank-Nicholson approximation (e.g., Press, et al., 1988, p. 658–661). Applying this scheme to the equations for p and q yields two equations with two unknowns, p^{j+1} and q^{j+1}:

$$\begin{aligned} q^{j+1} - q^j &= \left(\frac{\Delta t}{2}\right)\left[A^{j+1}p^{j+1} + A^j p^j\right], \\ p^{j+1} - p^j &= \left(\frac{\Delta t}{2}\right)\left[B^{j+1}q^{j+1} + B^j q^j\right], \end{aligned}$$

where $q^0 = 0$ and $p^0 = 1/v_0$, and the variables A^j, and B^j are defined by

$$A^j = (v^j)^2, \qquad B^j = v_{,zz}{}^j p_x^2 v^j.$$

Solving for p^{j+1} and q^{j+1} yields

$$\begin{aligned} q^{j+1} &= \frac{p^j}{\alpha}\left(\frac{\Delta t}{2}\right)\left[A^{j+1} + A^j\right] + \frac{q^j}{\alpha}\left[1 - \left(\frac{\Delta t}{2}\right)^2 A^{j+1}B^j\right], \\ p^{j+1} &= \frac{p^j}{\alpha}\left[1 - \left(\frac{\Delta t}{2}\right)^2 A^j B^{j+1}\right] - \frac{q^j}{\alpha}\left(\frac{\Delta t}{2}\right)\left[B^{j+1} + B^j\right], \end{aligned}$$

where α is defined by

$$\alpha = 1 + \left(\frac{\Delta t}{2}\right)^2 A^{j+1}B^{j+1}.$$

Dip-decomposition

From the finite difference solutions for σ and q, the dip-dependent divergence correction $\sqrt{\sigma q}$ is tabulated for all reflection times and all reflection slopes. The dip-dependent divergence correction is equivalent to a time-varying dip filter because of its simultaneous dependence on reflection slope and reflection time. Although dip-dependent processing is most easily implemented in the frequency-wavenumber domain, the time-dependent attributes of the table cannot be considered once the 2-D Fourier transform is made. To apply the divergence correction, I use a dip-decomposition technique similar to Jakubowicz's (1990) method for efficient DMO. For each reflection slope p_x and time t, the dip-dependent divergence correction is applied in the wavenumber-time domain. The dip-filtered data are then transformed to the wavenumber-frequency domain. In this domain, only the frequencies near the wavenumber-slope ratio $\omega = k/p_x$ are included in the divergence-corrected data $B(x,t)$. The dip-decomposition algorithm is summarized below:

Zero $B(k,\omega)$
Fourier transform the stacked data $a(x,t)$ to $A(k,t)$
For all wavenumbers k {
    For all slopes p_x {
        Apply the divergence correction for all times t so that:
            $s(k,t) = D(p_x,t) \times A(k,t)$
        Fourier transform $s(k,t)$ to $S(k,\omega)$
        For all frequencies ω near k/p_x {
            Add $S(k,\omega)$ to the output $B(k,\omega)$
        }
    }
}
Inverse Fourier transform $B(k,\omega)$ to give the divergence-corrected data $b(x,t)$.

The dip-decomposition algorithm efficiently applies the dip-dependent divergence correction to stacked data. For example, applying the dip-dependent divergence correction to a stacked data set of 800 traces, each with 750 time samples, took 1 minute and 20 s on an IBM RS/6000. Compare this time to the migration time – 90 minutes, using a time-wavenumber $t-k$ migration process (Hale, 1991). The dip-dependent divergence correction required only 1.5 % of the migration time.

To include the transmission factor in the algorithm described above, use the ray tracing equations (5) to compute $\sqrt{v_0/v(z)}$ at every point along the downgoing raypath as a function of reflection time and reflection slope. Then apply the full amplitude correction for both geometrical spreading and the transmission factor in place of the divergence correction. Given a velocity function that varies with depth and stacked data, the dip-decomposition algorithm is an efficient way to implement the dip-dependent amplitude correction.

DIVERGENCE CORRECTION RATIO

The importance of the dip-dependent divergence correction is evaluated by comparing amplitudes after conventional divergence correction to amplitudes after dip-dependent correction. For comparison, the conventional correction has been adjusted by a factor of two to correct for geometrical spreading only along the raypath *to* the reflection point. The dip-dependent divergence correction is compared to the conventional correction in contour plots of the ratio of conventional to dip-dependent correction. These contours show that the conventional divergence correction over-amplifies dipping reflections, and that the importance of dip-dependent divergence correction depends on reflection slope, reflection time, velocity function, and whether or not the transmission factor $\sqrt{v_0/v(z)}$ is required.

Horizontal and Dipping Reflectors

For interval-velocity functions that increase with depth, the geometrical spreading correction is largest for energy that travels the farthest and penetrates most deeply into the medium; i.e., at large times and at small values of horizontal slowness (reflection slope), where the direction of propagation is nearly vertical.

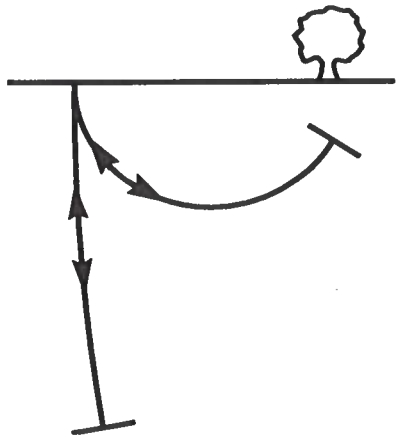

FIG. 4. A shallow, overhung reflector and a deep, nearly horizontal reflector in a medium where the velocity increases with depth. The reflection times of the two normal-incidence raypaths are equal. The divergence correction is greater for the nearly horizontal reflector than for the dipping reflector.

Consider a dipping reflector and a nearly horizontal reflector in a medium where the velocity increases monotonically with depth (Figure 4). If the reflection times to these reflectors along the normal-incidence raypaths are the same, the dipping reflector must be shallower than the nearly horizontal reflector. The velocity along the normal-incidence raypath to the dipping reflector is therefore less than that for the nearly horizontal reflector.

Recall that both components σ and q of the dip-dependent divergence correction $\sqrt{\sigma q}$ depend on velocity along the raypath. From the differential equations (17)

and (18), it is seen that σ and q at a particular point on a raypath depend on the integral of the velocity squared along the raypath with respect to the traveltime to that point. For a normal-incidence ray that remains at shallow zones characterized by small velocities, such as the ray to the dipping reflector in Figure 1, the dip-dependent divergence correction will be smaller than for a normal-incidence ray that travels through deeper zones characterized by higher velocities; i.e., the ray to the nearly horizontal reflector in Figure 4. Thus, for fixed reflection time, the divergence correction decreases as reflector dip, or reflection slope increases. The maximum value of the divergence correction occurs for zero reflection slope or for horizontal reflectors, where the conventional divergence correction $v_{\text{rms}}^2 t/v_0$ is valid.

Comparing dip-dependent to conventional correction, the difference between corrections increases with traveltime in a medium where the velocity increases monotonically with depth. Consider two normal-incidence raypaths with the same small reflection time to a dipping and a horizontal reflector. For early reflection times, both the dipping and horizontal reflector must be located at shallow depths, and the deeper zones with higher velocities encountered by the ray to the horizontal reflector have velocities not very different from those that characterize the shallow ray to the dipping reflector. The difference between divergence corrections along those shallow raypaths is small. At late reflection times, however, the reflectors may be located at very different depths. For these late times, the raypath to the horizontal reflector travels through zones with much higher velocities than those along the raypath to the dipping reflector.

Figure 5a shows contours of the ratio of conventional divergence correction to dip-dependent divergence correction, as a function of reflection time and slope for the velocity function $v = 1.5 + 0.6z$. These contours indicate the amount of amplitude error when the conventional divergence correction is applied to an event with a particular reflection slope and reflection time. From the above discussion, contours with large ratios, where the conventional divergence correction differs greatly from the dip-dependent correction, should correspond to large dips or large reflection slopes and late times.

In Figure 5a, conventional divergence correction exaggerates amplitudes by less than three percent for events whose reflection slope and reflection time fall above the contour labeled 1.03. For events that fall on the 2.25 contour, the conventional correction over-amplifies those events by approximately 125 percent. The amount of over-amplification after conventional divergence correction increases with reflection slope and reflection time.

Figure 5b corresponds to Figure 5a, but the ratio of divergence corrections is expressed as a function of reflector dip and vertical time. Whereas Figure 5a indicates the amount of over-amplification after conventional correction on a zero-offset section, Figure 5b shows amplitude error after conventional correction for a migrated section. For the velocity function $v = 1.5 + 0.6z$, the conventional divergence correction ex-

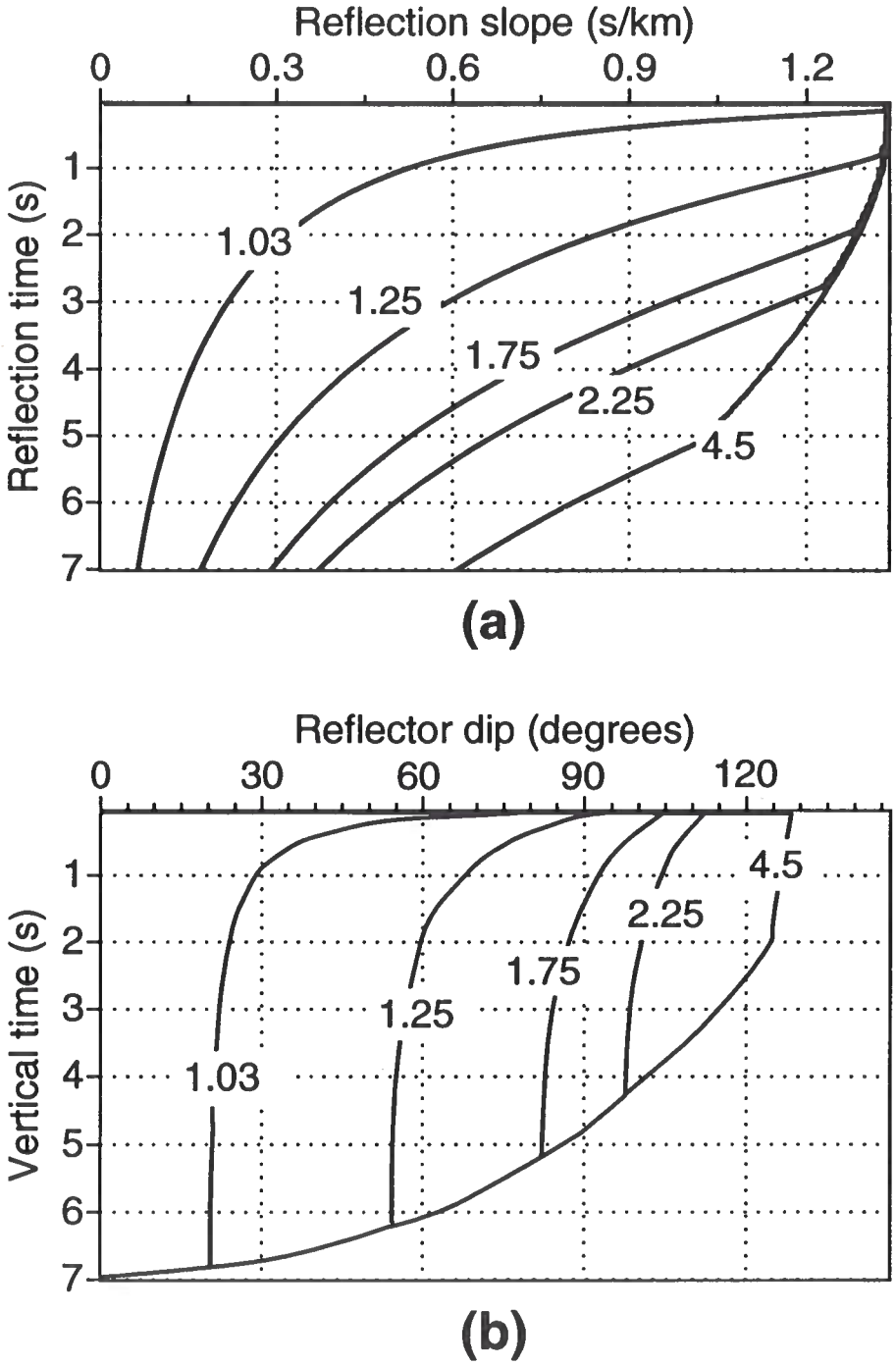

FIG. 5. (a) Contours of the ratio of conventional to dip-dependent divergence correction as a function of reflection slope and reflection time, in a medium with velocity function $v = 1.5+0.6z$ km/s. For events in a stacked section with reflection slopes and times that fall along a given contour, such as the 1.75 contour, the conventional correction over-amplifies dipping events by a factor of 1.75. (b) Corresponding contours as a function of reflector dip and vertical (migrated) time.

aggerates amplitudes by less than three percent for reflectors dipping at less than 20 degrees. Note that error increases with dip.

The error contours of Figure 5b converge at the bottom of the figure. The contours are bounded by the largest possible dips from which a normal-incidence ray in the $v = 1.5 + 0.6z$ medium can be reflected and recorded within the maximum recording time of 7 s.

Velocity Gradient

Figure 5 describes the amplitude error that results from applying the conventional divergence correction to dipping reflectors for a medium with velocity function $v = 1.5 + 0.6z$. If the velocity gradient is increased, the amplitude error in conventionally corrected data will become significant at smaller reflection slopes and earlier times. In other words, the amplitude error contours will migrate to the left, as in Figure 6a, where the velocity function equals $1.5 + 0.9z$. The error contours in Figure 6b reach later vertical (migrated) times than those in Figure 5b. This is because within the maximum recording time of 7 s, a normal-incidence ray in a medium with a high velocity gradient will reach greater depths and larger migrated times than a normal-incidence ray in a medium with a smaller velocity gradient.

A large velocity gradient will increase the velocity along a normal-incidence raypath, and thus magnify the *ratio* of conventional to dip-dependent divergence correction. Similarly, a small velocity gradient will diminish the difference between conventional and dip-dependent divergence correction. This is the case for the Gulf of Mexico velocity function. (See the section on Results, p. 27.)

Velocity Curvature

The dip-dependent divergence corrections depends on the curvature $v_{,zz}$ of the velocity function as well as the velocity gradient. For a velocity function with changes in the curvature $v_{,zz}$ (Figure 7a), the contours of amplitude error after conventional divergence correction (Figure 7c) are twisted relative to the smooth contours of a velocity function with zero curvature (Figure 5a). Note that the velocity function used in Figure 5a has constant gradient with respect to depth z, and thus zero curvature.

Recall that the curvature $v_{,zz}$ contributes to dip-dependent divergence correction $\sqrt{\sigma q}$ through the in-plane divergence factor q, given by equations (18). The differential equation for q is coupled to p, and the derivative of p with respect to traveltime is proportional to the curvature $v_{,zz}$. Changes in curvature $v_{,zz}$ affect both magnitude and sign of p. As the derivative of q with respect to traveltime is proportional to p, the changes in curvature $v_{,zz}$ will retard or accelerate increments in q. Because q at a given traveltime depends on velocity and p at earlier times along the ray, a change in curvature at a particular depth will affect not only p and q at that point along the raypath, but also later values of p and q.

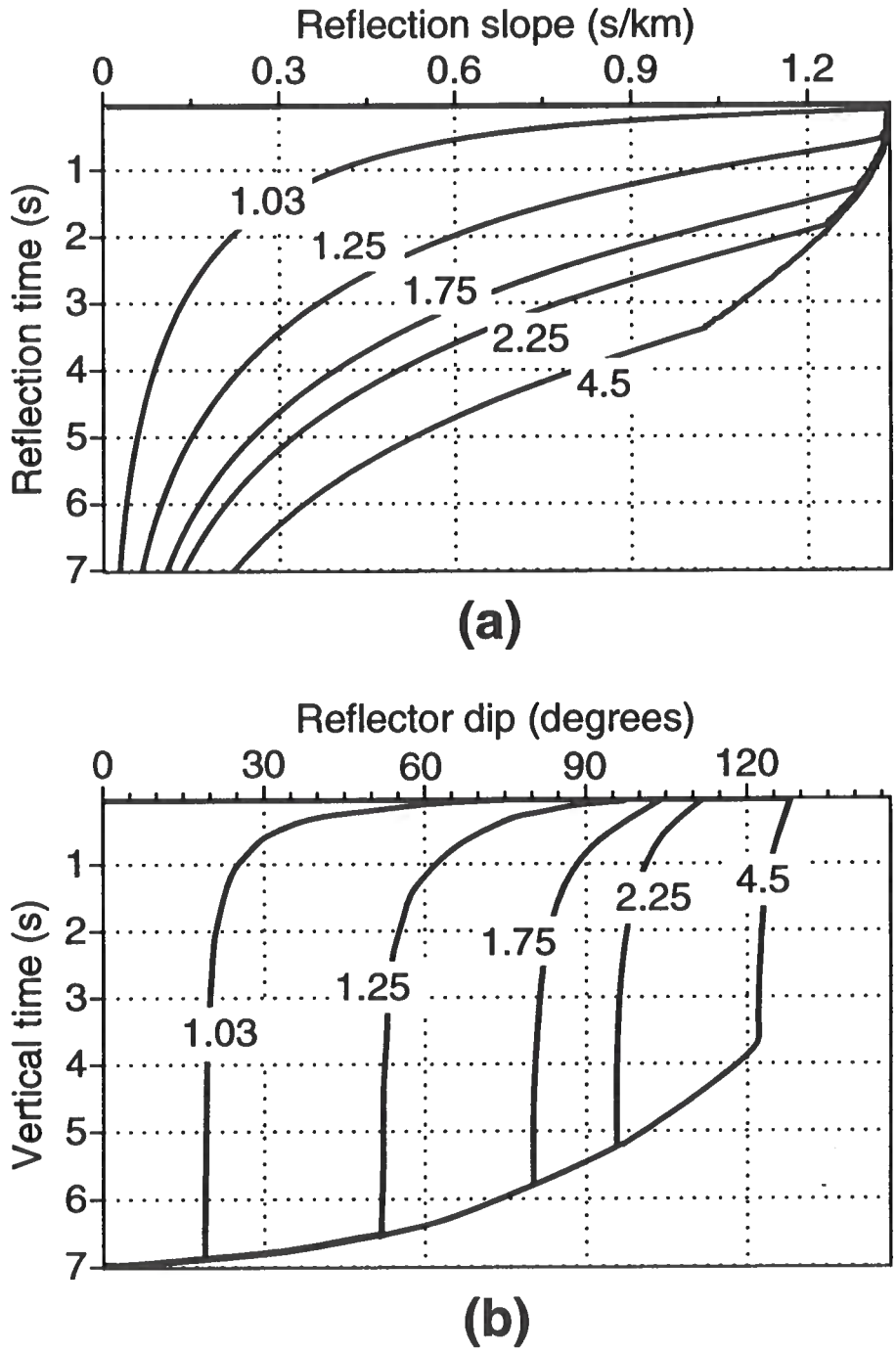

FIG. 6. (a) Contours of amplitude error after conventional divergence correction as a function of reflection slope and reflection time for a medium with velocity function $v = 1.5+0.9z$ km/s. Corresponding contours as a function of reflector dip and vertical (migrated) time. Compare with Figure 5.

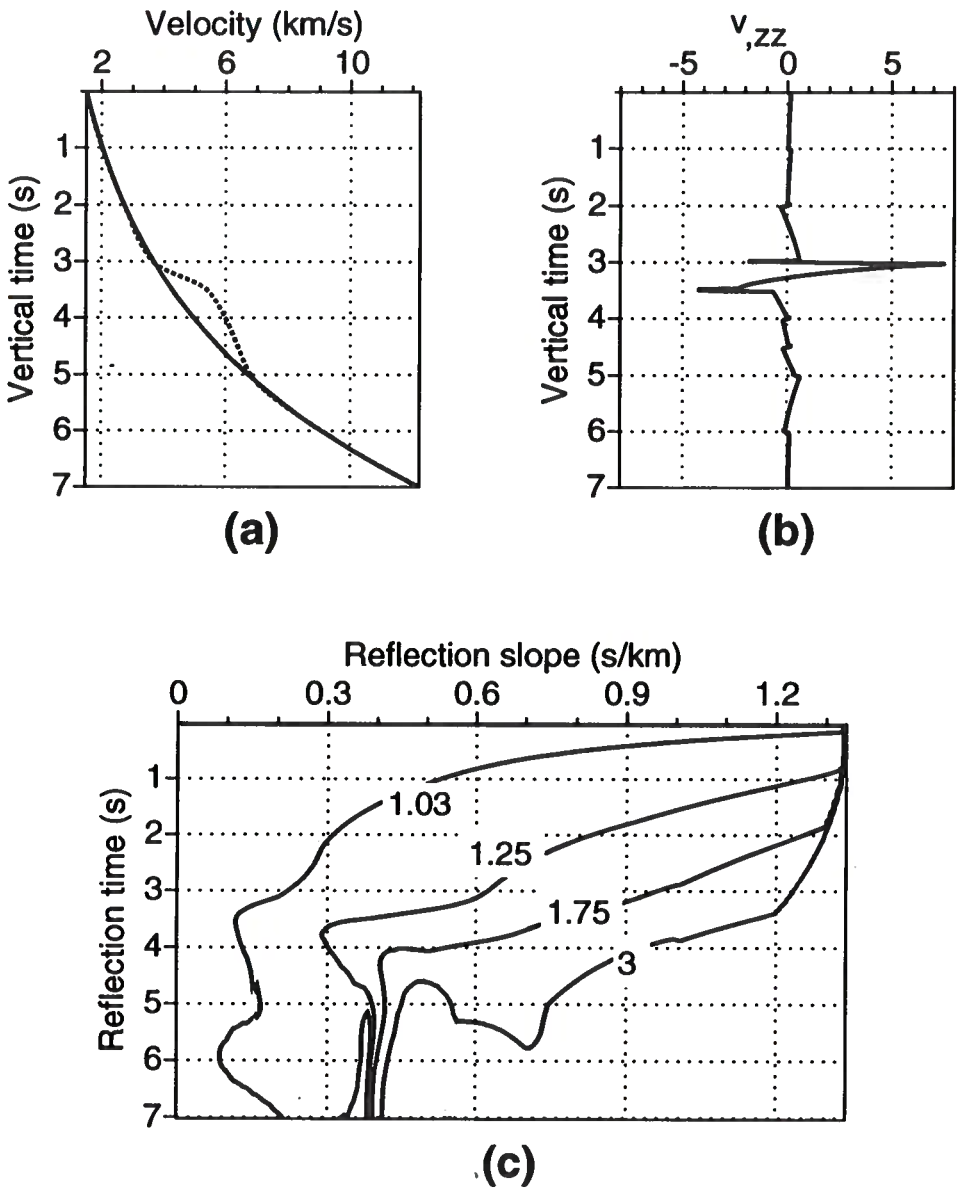

FIG. 7. (a) Two interval velocity functions. (b) Second derivative of the velocity function, given by the dashed line in (a), with respect to depth z as a function of vertical time τ; i.e., $v_{,zz}(\tau)$. (c) Amplitude error contours that result from applying the conventional divergence correction for a medium described by the interval velocity, given by the dashed line in (a). Compare the distorted contours in (c) with the contours in Figure 5a.

Two velocity functions are displayed in Figure 7a. The dashed line corresponds to the velocity function $v = 1.5+0.6z$. This function is linear with depth and exponential in vertical time; the curvature $v_{,zz}$ is zero. The velocity function described by the solid line includes a high-velocity zone between 3 and 5 s. This high-velocity zone introduces changes in curvature $v_{,zz}$, shown in Figure 7b. Just as velocity is given as a function of vertical time τ, the second derivative of velocity $v_{,zz}$ with respect to depth z is also given as a function of vertical time. The curvature $v_{,zz}$ as a function of vertical time τ is defined by the mapping:

$$v_{,zz}(\tau) = \frac{v_{,\tau\tau}}{v^2} - \frac{1}{v}\left(\frac{v_{,\tau}}{v}\right)^2.$$

For the velocity function given by the solid line in Figure 7a, there are two regions of large change in curvature $v_{,zz}(\tau)$; between 2.5 and 4 s, and around 5 s. Consider the 3% amplitude error contour of Figure 7c. The small reflection slopes that fall on this contour correspond to nearly horizontal reflectors, with nearly vertical normal-incidence raypaths. For these small reflection slopes, reflection time and vertical time are similar. The 3% amplitude error contour is strongly distorted with respect to the 3% error contour of Figure 5a between 2.5 and 4 s, and again around 5 s. This distortion correlates to the changes in curvature near those vertical times. For large reflection slopes and steep reflectors, the deformations in the amplitude error contours cannot be so easily correlated to changes in $v_{,zz}$ as a function of vertical time.

Transmission Factor

If after dip-dependent divergence correction, the data will be migrated with an exploding reflector migration scheme based on the *constant density* acoustic wave equation, then amplitudes after divergence correction will be consistent with exploding reflector data, *only* if the transmission factor is included.

Consider the dip-dependent divergence correction, when spreading $\sqrt{\sigma q}$ is multiplied by the transmission factor $\sqrt{v_0/v(z)}$. For a velocity function that increases monotonically with depth, as reflector depth increases the divergence correction increases; however, the transmission factor decreases. Amplitudes are less exaggerated after conventional correction when the transmission factor is included. With the transmission factor, the amount of over-amplification is significant only for large reflection slopes or steep reflectors, and late times.

Figure 8 shows contours of the ratio of conventional divergence correction to dip-dependent correction, when the transmission factor $\sqrt{v_0/v(z)}$ is included in both corrections. The contours for the same values of amplitude error as in Figure 5a are shifted to higher reflection slopes. An event with reflection slope of 0.75 s/km and reflection time of 3.5 s falls on the 75% error contour of Figure 5a, but the 25% error contour of Figure 8.

The amount of over-amplification for a particular event after conventional correction depends on reflection slope, reflection time, velocity, velocity curvature, and

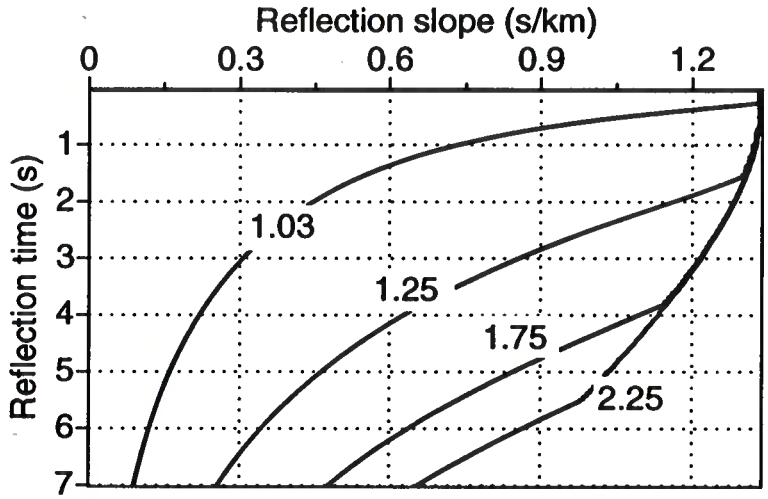

FIG. 8. Contours of amplitude error after conventional divergence correction, where the transmission factor $\sqrt{v_0/v(z)}$is included. The velocity function in the medium equals $1.5 + 0.6z$ km/s. Compare with Figure 5a.

whether or not the transmission factor is required. Figure 5 demonstrates that amplitude error increases with reflector dip and reflection slope. For large reflection slopes, the amount of over-amplification increases with reflection time. Amplitude error becomes significant at smaller reflection slopes and smaller reflection times if the velocity of the medium has a large gradient, as in Figure 6a. As well, amplitude error due to conventional divergence correction of a dipping event is sensitive to changes in velocity curvature $v_{,zz}$, as in Figure 7. Finally, Figure 8 demonstrated that with the transmission factor included, the amount of over-amplification after conventional divergence correction is decreased.

RESULTS

In the previous chapter, the dip-dependent divergence correction was compared to the conventional correction in contour plots of the ratio of conventional to dip-dependent correction. In this section, I show synthetic and field data examples of dip-dependent and conventional divergence-corrected data. Here, I compare the dip-dependent divergence-corrected data with the conventionally corrected data by taking the difference, i.e., subtracting the dip-dependent corrected data from the conventionally corrected data. The significance of the dip-dependent divergence correction is apparent when the amplitude difference is plotted at the same scale as the divergence-corrected data.

The amplitude difference, as shown in Figures 12 and 16, is evaluated *after* divergence-corrected data are migrated with an exploding reflector scheme. The data examples in this chapter have been migrated with a reverse time migration based on the *constant impedance* or non-reflecting acoustic wave equation. Amplitude, given by equation (9), in the constant impedance acoustic wave equation includes only a spreading term and no transmission factor. Consequently, the dip-dependent divergence correction applied to these data examples does *not* include the transmission factor.

The examples in Figures 10 through 16 demonstrate the amplitude effect of the dip-dependent divergence correction. In these examples, both conventional and dip-dependent divergence correction have been divided by the correction for zero slope at the first time sampling interval t_1: $v^2_{\text{rms}}(t_1)t_1/v_0$. This ensures that divergence correction is dimensionless, and is not a function of the units of velocity measurement.

The synthetic data were generated by a modeling program based on the 2.5-D Kirchhoff approximation (Bleistein, 1986). This program produced a zero-offset section, part of which is displayed in Figure 9. The data in this synthetic example as well as the field data example were migrated using a finite difference migration scheme (Hale, 1991). This migration process is implemented in the time-wavenumber $t-k$ domain, and yields amplitudes proportional to the reflection coefficients. Reflection coefficients of the model reflectors were constant throughout the model; within the limits of the modeling program, this constancy is preserved in the migrated dip-dependent divergence-corrected data of Figure 11b.

The reflection at 4.5 s with reflection slope of 0.75 s/km indicated by the arrow in Figure 9 corresponds to the steep reflector in the migrated data, Figure 11. The velocity function $v = 1.5 + 0.6z$ was used to generate the synthetic section. For this velocity, amplitude error after conventional correction applied to zero-offset data is contoured in Figure 5a. Note that the dipping event at 4.5 s falls on the 2.25 contour of Figure 5a; i.e, the conventional divergence correction will over-amplify that event by a factor of 2.25. Figures 10a and 10b show the synthetic stack after conventional and dip-dependent divergence correction respectively.

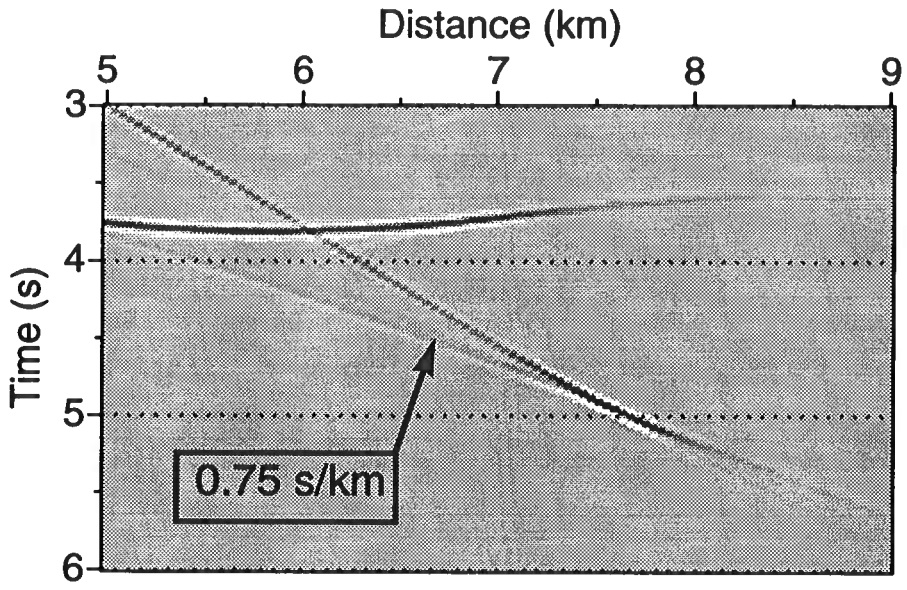

FIG. 9. Zero-offset synthetic data generated with interval velocity function $v = 1.5 + 0.6z$. No divergence correction has been applied. The amplitude error contours are those shown in Figure 5a. The dipping event at 4.5 s has a reflection slope of 0.75 s/km. This event falls on the 2.25 contour of Figure 5a.

Figure 11 displays the divergence-corrected stacked data of Figure 10 after migration. The contours of amplitude error after conventional divergence correction and migration are displayed as a function of reflector dip and vertical (migrated) time in Figure 5b. At a migrated time of 2.25 s, the steeply dipping reflector is overhung by about 7 degrees from the vertical. For a reflector with dip of 97 degrees and a migrated time of 2.25 s, Figure 5b indicates that the conventional divergence correction has over-amplified that reflector by 2.25 times.

Amplitudes in the dip-dependent divergence-corrected data of Figure 11b correspond to the interface reflection coefficients of the synthetic model, within the limits of the modeling program. Note that amplitudes in Figure 11b are nearly constant with a small increase in amplitude with depth. This amplitude increase with depth is an artifact of the modeling program. Although the reflection coefficients in the synthetic model were constant; the zero-offset amplitudes generated by the modeling program correspond to reflection coefficients that increase slightly with depth. Consequently, the dip-dependent divergence-corrected amplitude of the shallow horizontal reflector is 5% less than that of the deeper horizontal reflector.

The difference plot in Figure 12 demonstrates that the conventional divergence correction has exaggerated the amplitudes of dipping reflections. For nearly horizontal

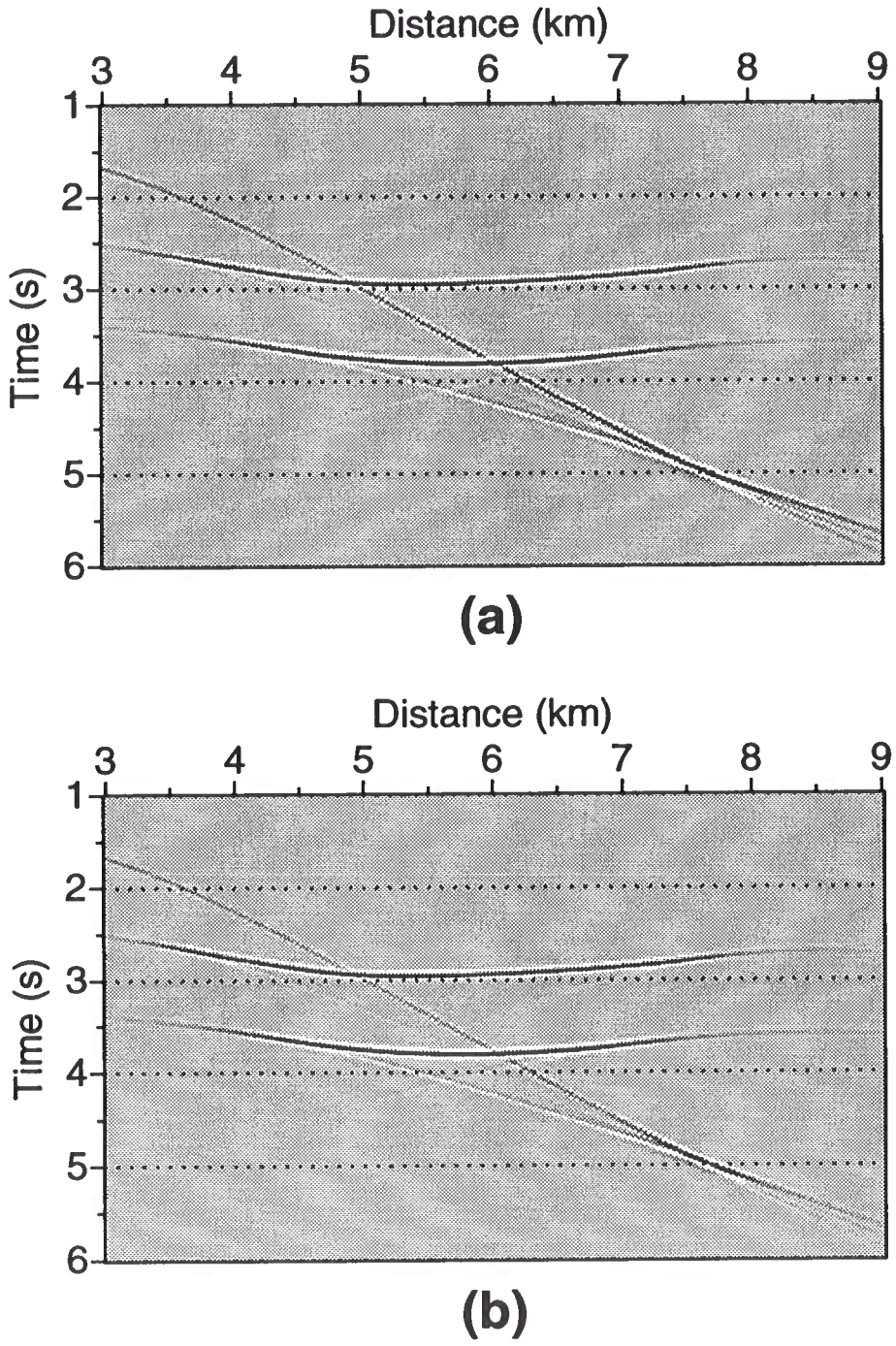

FIG. 10. (a) The synthetic stack with conventional divergence correction applied. (b) With dip-dependent divergence correction applied. The amplitudes of the steep reflection are stronger in the conventionally corrected data.

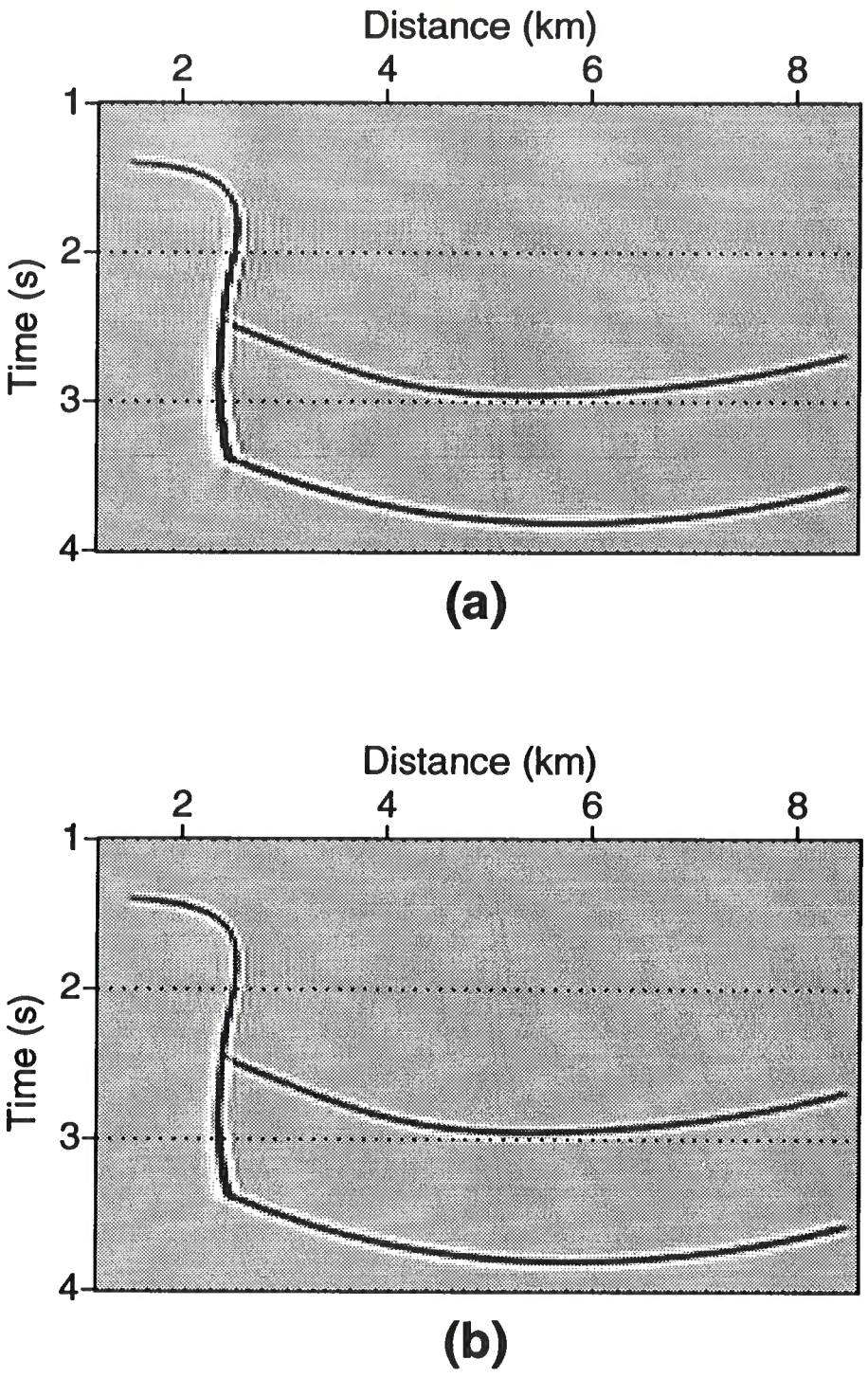

FIG. 11. (a) Migration of conventionally divergence-corrected data. (b) Migration of dip-dependent divergence-corrected data. Compare the amplitudes of the steep reflector.

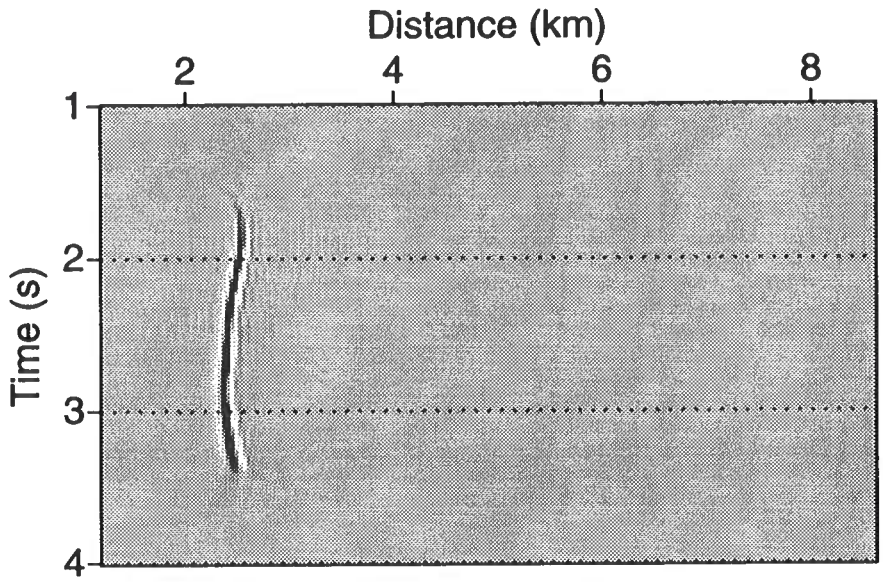

FIG. 12. The post-migration difference: conventionally corrected amplitudes minus dip-dependent divergence-corrected amplitudes.

reflectors, the dip-dependent divergence correction and the conventional divergence correction have the same action.

The dip-dependent divergence correction is applied to a Gulf of Mexico seismic line. In the Gulf of Mexico, an interval velocity function that varies with depth is a good approximation to the velocity of sediments through which seismic waves propagate. The arrow on the stacked data, Figure 13a, points to the salt flank reflection, with a reflection slope of 0.98 s/km at a time of about 3.5 s. This event falls on the 1.6 contour of Figure 14a. The conventionally corrected amplitudes along the salt flank are thus over-amplified by 60 percent.

In Figure 15, I compare the migrated conventionally corrected field data to the migrated dip-dependent divergence-corrected field data. As for the synthetic example, amplitudes of migrated reflections from the steep beds are brighter on the conventionally corrected data, although the difference as shown in Figure 16 is more subtle here.

Figure 16 shows that the conventional correction has also over-amplified the dipping interface at the crown of the salt dome, about 1.7 s. These interfaces dip at an angle of about 45 degrees, and from Figure 14b, the conventional correction will have over-amplified these reflections by a factor of about 1.1. Because this reflector has a relatively high amplitude, its small 10% error in amplitude after conventional correction shows on the difference plot of Figure 16.

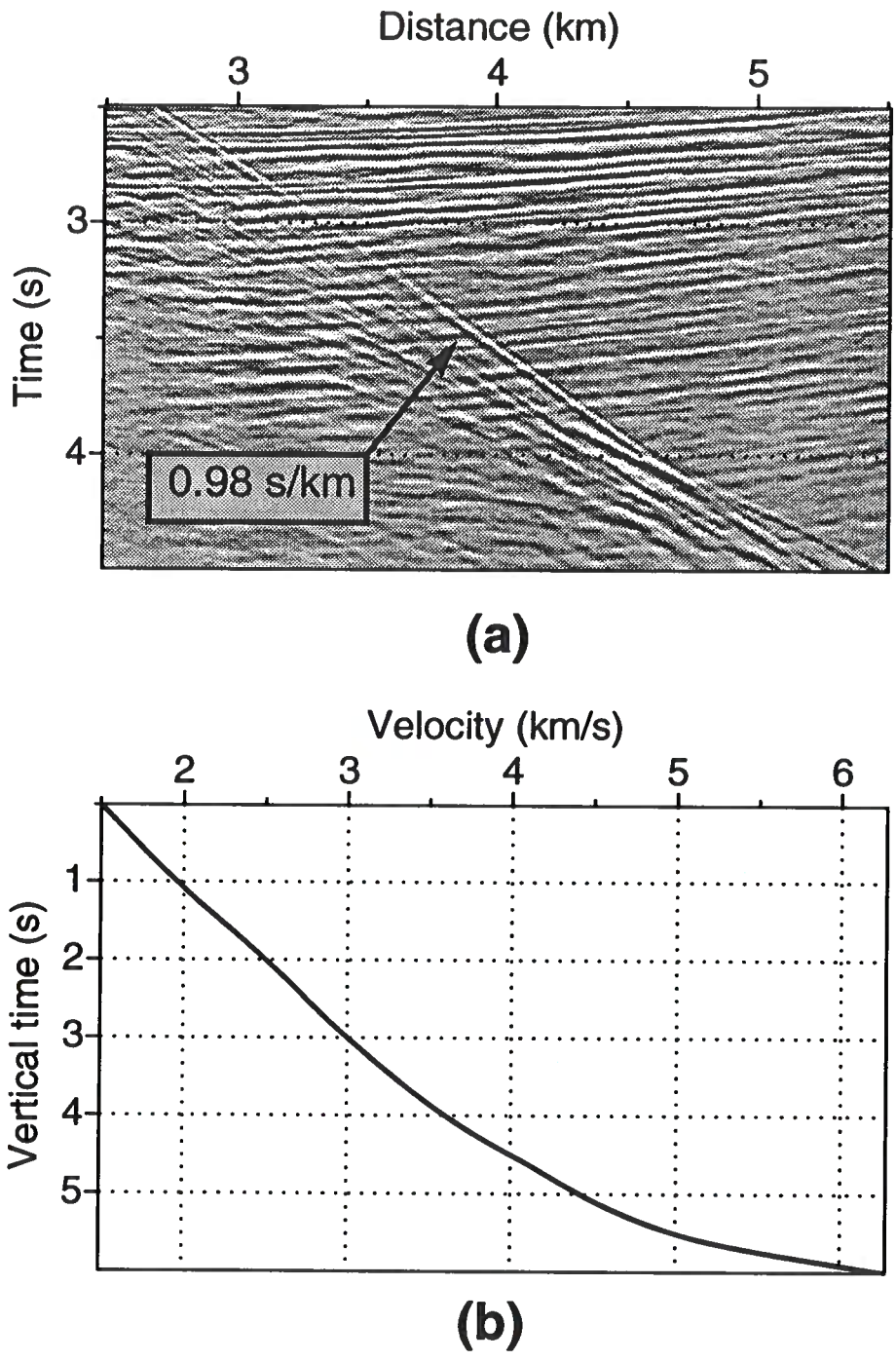

FIG. 13. (a) A part of the field data stack without divergence correction showing the dipping events that correspond to the salt flank. The dipping event at 3.5s has a reflection slope of 0.98 s/km. This event falls on the 1.6 contour of Figure 14a. (b) Interval velocity used to migrate the field data.

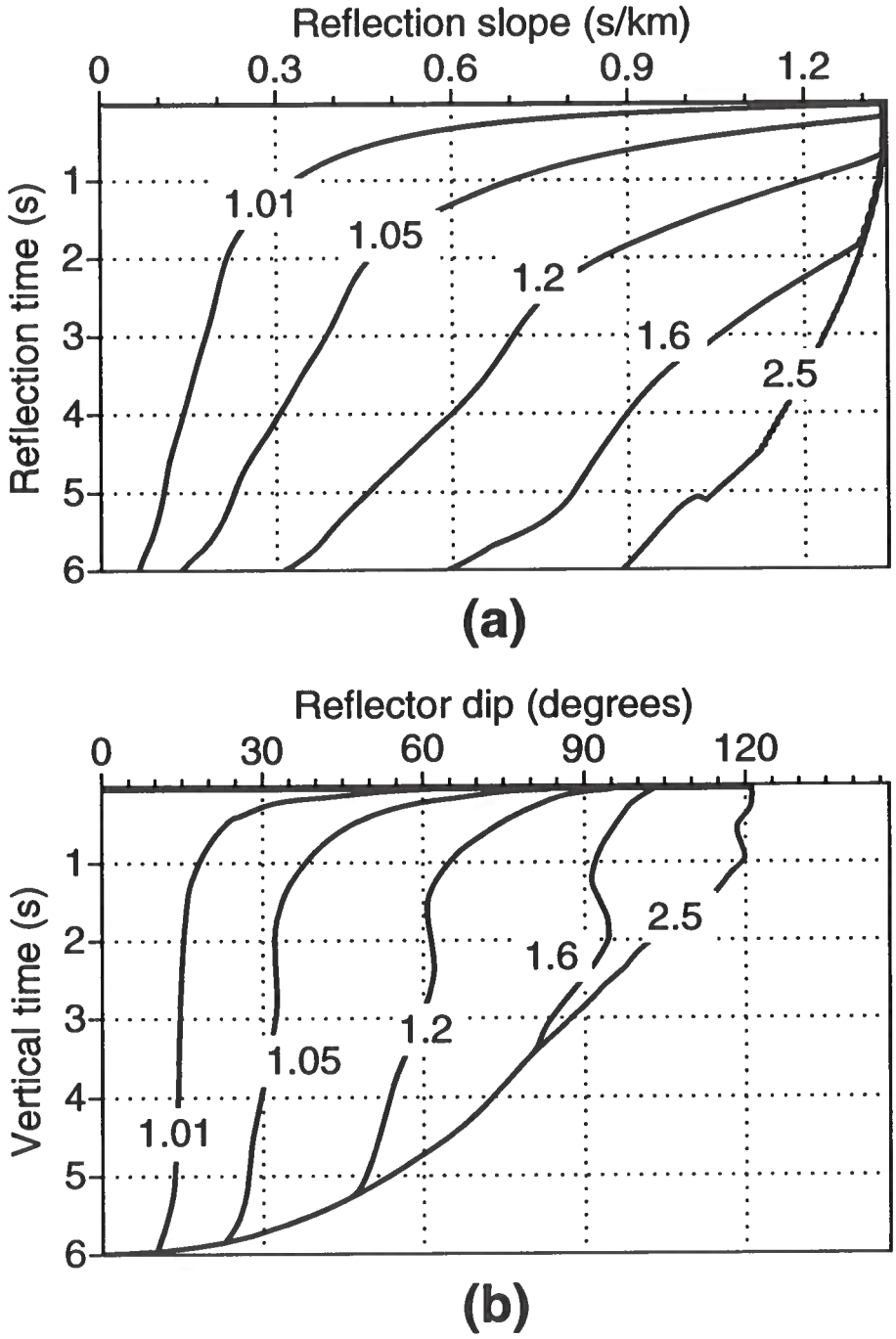

FIG. 14. (a) Contours of the ratio of conventional to dip-dependent divergence correction as a function of reflection slope and reflection time. (b) Corresponding contours as a function of reflector dip and vertical time. The velocity model is shown in Figure 13b.

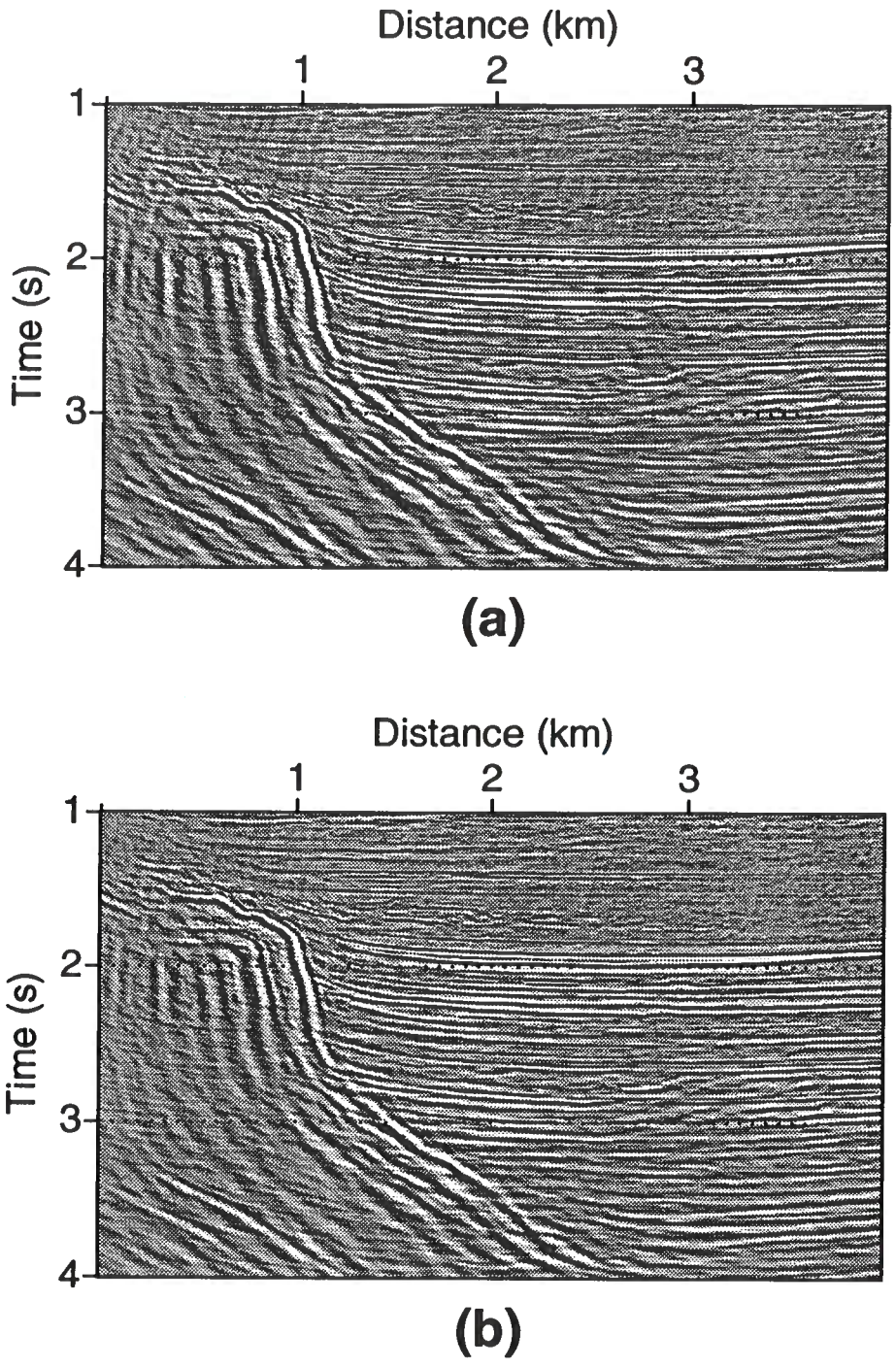

FIG. 15. (a) Migration of conventionally divergence-corrected data. (b) Migrated data with amplitudes adjusted by the dip-dependent divergence correction.

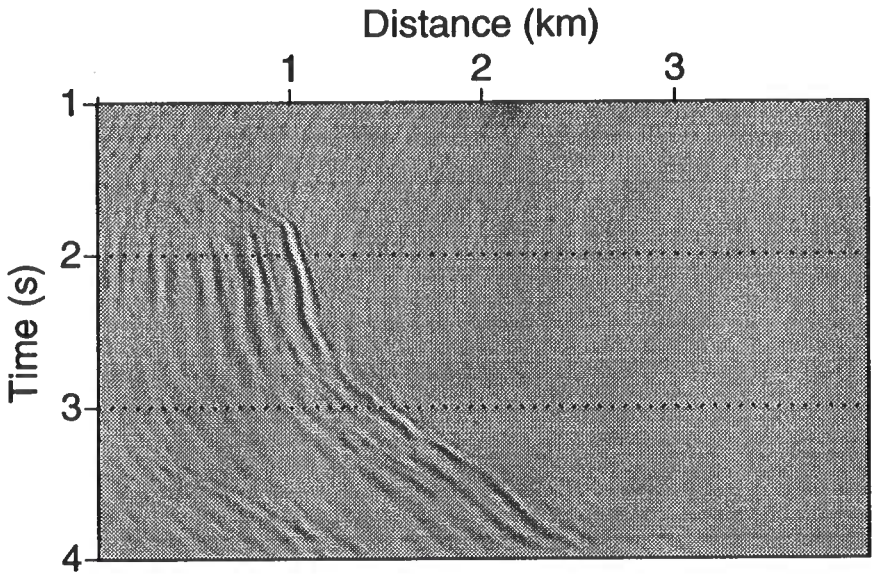

FIG. 16. The post-migration difference: conventionally corrected amplitudes minus dip-dependent divergence-corrected amplitudes.

The velocity increase in the Gulf of Mexico data is less rapid here than in the synthetic model studied above, therefore the amplitude difference in Figure 16 is less dramatic than for the synthetic example. In this medium, the conventional divergence correction is valid over a larger range of dips and traveltimes. As before, the dip-dependent divergence correction has decreased the amplitudes of dipping beds relative to the conventional divergence correction, and the amount of over-amplification after conventional correction increases with reflector dip.

CONCLUSION

The poststack dip-dependent divergence correction compensates for amplitude decay due to geometrical spreading in a $v(z)$ medium. It is designed to correct the zero-offset amplitudes of a 2-D seismic line oriented in the direction of geological dip. After application of the dip-dependent divergence correction, amplitudes in zero-offset data will be consistent with the exploding reflector model. If an exploding reflector migration that treats amplitudes in accordance with the acoustic wave equation, i.e., reverse time migration, is then applied to the divergence-corrected data, then the migrated amplitudes will be more interpretable in terms of interface reflection coefficients, than if the conventional divergence correction had been applied.

The error in amplitude due to the conventional divergence correction is most significant for events with large reflection slope at late times. For the field data example from the Gulf of Mexico shown in the previous section, the conventional divergence correction over-amplified dipping events by as much as 60 percent.

The dip-dependent divergence correction improves the amplitude processing of dipping reflectors in a medium where the velocity varies only with depth. Gulf of Mexico data, which often contain steep reflectors and where the velocity profiles have little lateral variation, are particularly suited for the application of this correction.

For dipping beds with large reflection coefficients, the difference in amplitude after dip-dependent divergence correction may be dramatic. Where the conventional correction would introduce 'bright spots' in such beds, amplitudes in the migrated dip-dependent divergence-corrected data are more closely related to the interface reflection coefficients. Note that for dipping beds that do contain 'bright spots', dip-dependent divergence correction preserves the relative brightness.

Although the dip-dependent divergence correction has been applied to 2D zero-offset sections in this thesis; it is a simple matter to extend the correction for 3D data sets. Just as the downward continuation operator is extended to 3D migration schemes by considering the magnitude of the horizontal wavenumber, the dip-dependent divergence correction may be extended to 3D by replacing the horizontal slowness p_x in the x direction with the magnitude of the horizontal slowness vector $\sqrt{p_x^2 + p_y^2}$, where p_y is the horizontal slowness in the y direction.

To correct for dip-dependent divergence in finite-offset data, the dip-dependent correction must compensate for geometrical spreading along *both* the raypath from shot to reflection point *and* along the raypath from reflection point to receiver. As discussed in the introduction, such a divergence correction would require two-point ray tracing to determine the traveltimes and horizontal slownesses of the incident and reflected rays associated with each finite-offset reflection. Furthermore, while the divergence correction for the incident raypath may be tabulated as a function of horizontal slowness, and traveltime; the divergence correction for the reflected raypath must be tabulated for every reflection point, horizontal slowness, and traveltime.

Clearly, dip-dependent divergence correction for finite-offset data would be an expensive process in terms of the ray tracing necessary to determine the reflection point and the appropriate divergence correction for every finite-offset reflection from that point. The finite-offset dip-dependent divergence correction and its implementation require further study; however, I expect that the amplitude effects of the dip-dependent divergence correction applied to finite-offset data, which are subsequently stacked, will not differ significantly from those of the poststack divergence correction.

To see this, consider a dipping reflector in a constant velocity medium, with velocity v_0. The divergence correction along the incident raypath will equal the total distance along that raypath: $v_0 t_i$, where t_i is the traveltime to the reflection point. Similarly, the divergence correction for the reflected raypath will be $v_0 t_r$, where t_r is the traveltime to the reflection point. The total divergence correction will equal $v_0(t_i + t_r) = v_0 t$, where t is the reflection time. Except for a factor of two to account for the exploding reflector model, this divergence correction $v_0 t$ is identical to the poststack divergence correction for a constant velocity medium. Admittedly, the divergence correction is more complicated for a $v(z)$ medium; however, the averaging effect seen in the constant velocity case will also occur in the $v(z)$ medium; and consequently, I do not expect a significant improvement in amplitude processing to result from extending the dip-dependent divergence correction to finite-offset data.

Acknowledgments

I thank my advisor, Dr. Dave Hale, for suggesting this thesis topic and for providing me with invaluable guidance and assistance.

The financial support of this project is provided by the Consortium Project on Seismic Inverse Methods for Complex Structures at the Center for Wave Phenomena (CWP), at the Colorado School of Mines. I thank my fellow researchers in CWP for their encouragement and helpful discussions.

This project is also supported by the United States Department of Energy, grant number DE-FG02-89ER14079. (This support does not constitute an endorsement by DOE of the views expressed in this paper.)

References

Aki, K., and Richards, P., 1980, Quantitative seismology: Vol 1, W.H. Freeman and Company.

Baysal, E., Kosloff, D, and Sherwood, J., 1983, Reverse time migration: Geophysics, **48**, 1514-1524.

Baysal, E., Kosloff, D, and Sherwood, J., 1984, A two-way non-reflecting wave equation: Geophysics, **49**, 132–141.

Bleistein, N., 1986, Two-and-one-half dimensional in-plane wave propagation: Geophys. Prosp., **34**, 686–703.

Bleistein, N., 1984, Mathematical methods for wave phenomena: Academic Press, Inc.

Červený, V., 1981a, Ray tracing in a vicinity of a central ray: Stanford Exploration Project, **28**, 39–48.

Červený, V., 1981b, Computation of geometrical spreading by dynamic ray tracing: Stanford Exploration Project, **28**, 49–59.

Červený, V., and Hron, F., 1980, Ray series method and dynamic ray tracing system for three-dimensional inhomogeneous media: Bul. Seis. Soc., **70**, 47–77.

Červený, V., and Ravindra R., 1971, Theory of seismic head waves: University of Toronto Press.

Červený, V., Molotkov, I. A., and Pšenčik, I., 1977, Ray method in seismology: Univerzita Karlova Praha.

Gazdag, J., 1978, Wave equation migration with the phase shift method: Geophysics, **43**, 1342–1351.

Hubral, P., 1983, Computing true amplitude reflections in a laterally inhomogenous earth: Geophysics, **48**, 1051–1062.

Jakubowicz, H., 1990, A simple efficient method of dip-moveout correction: Geophys. Prosp., **38**, 221–245.

Loewenthal, D., Lu, L., Robertson, R., and Sherwood, J., 1976, The wave equation applied to migration: Geophys. Prosp., **24**, 380–399.

Newman, P., 1973, Divergence effects in a layered earth: Geophysics, **38**, 481–488.

Press, W., Flannery, B., Teukolsky S., and Vetterling, 1988, Numerical Recipes in C: Cambridge University Press.

Towne, D. H., 1967, Wave Phenomena: Addison-Wesley Publishing Company.

Appendix A

THE TRANSMISSION FACTOR

In this appendix, I justify my identification of the velocity ratio $\sqrt{v_2/v_1}$ as the transmission factor. Transmission coefficients and amplitude losses due to transmission are defined in a medium with interfaces across which the velocity function $v(z)$ changes discontinuously. However, the dip-dependent divergence correction was derived for a continuous medium. Strictly speaking, no amplitude losses due to transmission may occur in the continuous model used for the dip-dependent divergence correction. However, the continuous $v(z)$ medium where velocity v varies with depth z only may be modelled by a series of constant velocity horizontal layers in the limit, as the change in velocity between the layers goes to zero. I consider the amplitude change across a single interface in the layered medium. Across this interface, velocity changes from v_1 to v_2. For the limit in which the discrete medium with transmission effects equals the continous medium, I show that the change in amplitude across this interface is independent of angle of incidence and is simply $\sqrt{v_2/v_1}$.

The amplitude change across any interface is the product of incident amplitude, transmission *coefficient* of the interface, and change in geometrical spreading of the ray tube across the interface. First consider the transmission coefficient.

Transmission

The transmission coefficient (Towne, 1967, p. 411–417) across a single horizontal interface for an acoustic plane wave travelling in a constant density medium is

$$\mathrm{T} = \frac{2v_2 \cos\theta_1}{v_2 \cos\theta_1 + v_1 \cos\theta_2}. \tag{A-1}$$

The subscript 1 refers to quantities in the incident layer and 2 refers to quantities in the refracted layer. The angles θ_1 and θ_2 are, respectively, the angles of incidence and transmission with respect to the normal to the interface; see Figure A-1. The change in velocity Δv between the layers is defined by

$$\Delta v \equiv v_2 - v_1. \tag{A-2}$$

Similarly the change in angle $\Delta\theta$ between the layers is defined by

$$\Delta\theta \equiv \theta_2 - \theta_1. \tag{A-3}$$

To evaluate the transmission coefficient in the limit as Δv goes to zero, expand v_2 and $\cos\theta_2$ in terms of Δv, v_1, $\Delta\theta$ and $\cos\theta_1$. From equation (A-2), $v_2 = v_1 + \Delta v$. The Taylor series expansion of $\cos\theta_2$ gives the two-term approximation

$$\cos\theta_2 \simeq \cos\theta_1 + \Delta\theta(-\sin\theta_1). \tag{A-4}$$

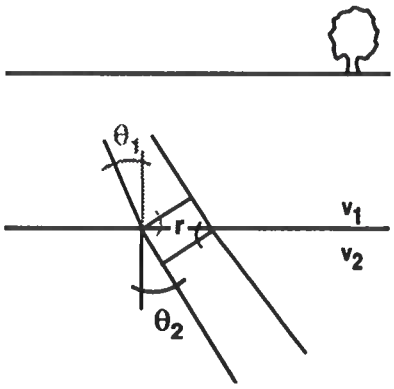

FIG. A-1. Transmission across a single interface in a discretized $v(z)$ medium. The ray tube is shown incident on and refracted from the interface. The spreading, or breadth of the ray tube is measured along the perpendicular line that connects the exterior rays of the ray tube. r is the horizontal width of the raytube along the interface. The two angles marked in gray are equal to θ_1, the angle made by the normal to the incident wavefront with respect to the vertical. Similarly, the two angles marked in black are equal to θ_2.

No further terms in the expansion are necessary, because $\Delta\theta$ is of order Δv, as shown below. Angles of incidence and refraction are related to velocity by Snell's law

$$\frac{\sin\theta_1}{v_1} = \frac{\sin\theta_2}{v_2}.$$

Replacing $\sin\theta_2$ by the first two terms of its Taylor series expansion yields

$$\frac{\sin\theta_1}{v_1} \simeq \frac{\sin\theta_1 + \Delta\theta(\cos\theta_1)}{v_1 + \Delta v}.$$

Multiplication by $v_2/\sin\theta_1$ gives

$$\frac{v_2}{v_1} = 1 + \frac{\Delta v}{v_1} \simeq 1 + \Delta\theta(\cot\theta_1), \tag{A-5}$$

from which it follows that

$$\Delta\theta \simeq \frac{\Delta v}{v_1}\tan\theta_1. \tag{A-6}$$

For $\theta_1 < \pi/2$, $\Delta\theta$ is thus proportional to Δv. As Δv approaches zero, so does $\Delta\theta$, at the same rate.

Using equation (A-4) in the expression for transmission coefficient and substituting for v_2 yields

$$\mathrm{T} \simeq \frac{2(v_1 + \Delta v)\cos\theta_1}{(v_1 + \Delta v)\cos\theta_1 + v_1(\cos\theta_1 - \Delta\theta\sin\theta_1)}.$$

Dividing both numerator and denominator by $2v_1 \cos\theta_1$ gives

$$\begin{aligned} \mathrm{T} &\simeq \frac{1 + \Delta v/v_1}{\frac{1}{2}(1 + \Delta v/v_1) + \frac{1}{2}(1 - \Delta\theta \tan\theta_1)} \\ &= \frac{1 + \Delta v/v_1}{1 + (\Delta v/2v_1) - (\Delta\theta \tan\theta_1/2)}. \end{aligned}$$

The transmission coefficient can be written as $(1 + \Delta v/v_1)(1 + x)^{-1}$ where x is equal to the sum of the Δv and $\Delta\theta$ terms. In the limit as Δv and consequently $\Delta\theta$ go to zero, $x \ll 1$ and

$$(1 + x)^a \simeq 1 + ax. \tag{A-7}$$

With the approximation of equation (A-7), the transmission coefficient is thus

$$\begin{aligned} \mathrm{T} &\simeq \left(1 + \frac{\Delta v}{v_1}\right)\left(1 - \frac{\Delta v}{2v_1} + \frac{\Delta\theta \tan\theta_1}{2}\right) \\ &\simeq 1 + \frac{\Delta v}{2v_1} + \frac{\Delta\theta \tan\theta_1}{2}, \end{aligned} \tag{A-8}$$

when terms of higher order than Δv are neglected. Applying equation (A-7) a second time, the transmission coefficient may be rewritten as a square root

$$\mathrm{T} \simeq \left(1 + \frac{\Delta v}{v_1} + \Delta\theta \tan\theta_1\right)^{1/2}. \tag{A-9}$$

This result for the transmission coefficients is equivalent to the expansion of $\sqrt{v_2/v_1}\sqrt{\cos\theta_1/\cos\theta_2}$, also in the limit as Δv goes to zero. To see this, start with

$$\sqrt{\frac{v_2}{v_1}}\sqrt{\frac{\cos\theta_1}{\cos\theta_2}} \simeq \left[\frac{(v_1 + \Delta v)\cos\theta_1}{v_1(\cos\theta_1 - \Delta\theta \sin\theta_1)}\right]^{1/2}.$$

Dividing both numerator and denominator on the right side by $v_1 \cos\theta_1$ yields

$$\begin{aligned} \sqrt{\frac{v_2}{v_1}}\sqrt{\frac{\cos\theta_1}{\cos\theta_2}} &\simeq \left(\frac{1 + \Delta v/v_1}{1 - \Delta\theta \tan\theta_1}\right)^{1/2} \\ &\simeq \left[\left(1 + \frac{\Delta v}{v_1}\right)(1 + \Delta\theta \tan\theta_1)\right]^{1/2} \qquad \text{(A-10)} \\ &\simeq \left(1 + \frac{\Delta v}{v_1} + \Delta\theta \tan\theta_1\right)^{1/2}. \qquad \text{(A-11)} \end{aligned}$$

The approximation of equation (A-7) was used to obtain (A-10), and terms of higher order than Δv were neglected to obtain (A-11).

The right side of equation (A-11) is identical to that of equation (A-9). Therefore the transmission coefficient for a wavefront incident upon a horizontal boundary in the limit as the velocity difference Δv goes to zero is

$$\mathrm{T} \simeq \sqrt{\frac{v_2}{v_1}}\sqrt{\frac{\cos\theta_1}{\cos\theta_2}}. \tag{A-12}$$

Note that for normal-incidence, $\theta_1 = \theta_2 = 0$, and the transmission coefficient T reduces to $\sqrt{v_2/v_1}$.

Spreading

The change in spreading of a ray tube across an interface is also angularly dependent. Figure A-1 relates the spreading dS_1 of the incident ray tube, to the spreading dS_2 of the refracted ray tube. The breadth of the ray tube is defined by the angle θ and horizontal width of the ray tube along the interface, r. Thus the breadth (perpendicular width) of the incident ray tube is

$$dS_1 = r\cos\theta_1.$$

Similarly, the breadth of the transmitted ray tube is

$$dS_2 = r\cos\theta_2$$

Eliminating r from these equations yields

$$\frac{dS_2}{dS_1} = \frac{\cos\theta_2}{\cos\theta_1}. \tag{A-13}$$

The ratio of refracted to incident breadth defines the change in geometrical spreading across an interface. Note that this accounts for only a part of the divergence; because geometrical spreading also occurs as the ray tube travels within the constant velocity layers.

The amplitude A_2 of the refracted ray tube is the product of the incident amplitude A_1, the change in geometrical spreading, and the transmission coefficient. The change in geometrical spreading across the interface is given by equation (A-13). Equation (A-12) describes the transmission coefficient. If A_1 is the amplitude just above a horizontal interface, then the amplitude A_2 just below the interface is:

$$\begin{aligned} A_2 &= A_1 \times \sqrt{\frac{dS_2}{dS_1}} \times \mathrm{T} \\ &= A_1\sqrt{\frac{\cos\theta_2}{\cos\theta_1}}\sqrt{\frac{v_2}{v_1}}\sqrt{\frac{\cos\theta_1}{\cos\theta_2}} \\ &= A_1\sqrt{\frac{v_2}{v_1}}. \end{aligned} \tag{A-14}$$

The change in amplitude across a single interface is equal to the normal-incidence transmission coefficient $\sqrt{v_2/v_1}$, what I have called the transmission *factor*. For many layers, the change in amplitude across the layer interfaces is

$$\sqrt{\frac{v(z)}{v_0}} = \sqrt{\frac{v_1}{v_0}} \times \sqrt{\frac{v_2}{v_1}} \times \ldots \times \sqrt{\frac{v(z)}{v(z-\Delta z)}}.$$

Both the transmission coefficient and the discontinuity in the spreading across an interface are functions of the angle of incidence. As equation (A-14) illustrates, this angular dependence cancels across an interface, thus leaving only $\sqrt{v_2/v_1}$, or the more general $\sqrt{v(z)/v_0}$, as the transmission *factor*.